

Article

Potent and Selective Human Neuronal Nitric Oxide Synthase Inhibition by Optimization of the 2-Aminopyridine-based Scaffold with a Pyridine Linker

Heng-Yen Wang, Yajuan Qin, Huiying Li, Linda J. Roman,
Pavel Martásek, Thomas L. Poulos, and Richard B. Silverman

J. Med. Chem., **Just Accepted Manuscript** • DOI: 10.1021/acs.jmedchem.6b00273 • Publication Date (Web): 06 Apr 2016

Downloaded from <http://pubs.acs.org> on April 7, 2016

Just Accepted

“Just Accepted” manuscripts have been peer-reviewed and accepted for publication. They are posted online prior to technical editing, formatting for publication and author proofing. The American Chemical Society provides “Just Accepted” as a free service to the research community to expedite the dissemination of scientific material as soon as possible after acceptance. “Just Accepted” manuscripts appear in full in PDF format accompanied by an HTML abstract. “Just Accepted” manuscripts have been fully peer reviewed, but should not be considered the official version of record. They are accessible to all readers and citable by the Digital Object Identifier (DOI®). “Just Accepted” is an optional service offered to authors. Therefore, the “Just Accepted” Web site may not include all articles that will be published in the journal. After a manuscript is technically edited and formatted, it will be removed from the “Just Accepted” Web site and published as an ASAP article. Note that technical editing may introduce minor changes to the manuscript text and/or graphics which could affect content, and all legal disclaimers and ethical guidelines that apply to the journal pertain. ACS cannot be held responsible for errors or consequences arising from the use of information contained in these “Just Accepted” manuscripts.

1
2
3
4 **Potent and Selective Human Neuronal Nitric Oxide Synthase Inhibition by**
5 **Optimization of the 2-Aminopyridine-based Scaffold with a Pyridine Linker**
6
7

8
9
10 Heng-Yen Wang,^{†,‡,¥} Yajuan Qin,^{†,‡,¥} Huiying Li,[§] Linda J. Roman,[¶] Pavel Martásek,^{¶,£,#}
11 Thomas L. Poulos,^{§,*} and Richard B. Silverman^{†,*}
12
13

14
15
16 †Department of Chemistry, Department of Molecular Biosciences, Chemistry of Life
17 Processes Institute, Center for Molecular Innovation and Drug Discovery, Northwestern
18 University, 2145 Sheridan Road, Evanston, Illinois 60208-3113, United States.
19
20

21
22 ‡State Key Laboratory of Pharmaceutical Biotechnology, School of Life Sciences, Nanjing
23 University, Nanjing 210093, People's Republic of China.
24
25

26
27 §Departments of Molecular Biology and Biochemistry, Pharmaceutical Sciences, and
28 Chemistry, University of California, Irvine, California 92697-3900, United States.
29
30

31
32 ¶Department of Biochemistry, University of Texas Health Science Center, San Antonio,
33 Texas 78384-7760, United States;
34

35
36 £Department of Pediatrics, First Faculty of Medicine, Charles University, Prague, Czech
37 Republic
38

39 # BIOCEV, Prague, Czech Republic
40

41 ¥ These author contributed equally.
42
43
44

45 **Keywords:** nitric oxide synthase, neurodegenerative diseases, mutant nNOS, human nNOS,
46 human eNOS, selective inhibition
47
48
49
50
51
52
53
54
55
56
57
58
59
60

Abstract

Neuronal nitric oxide synthase (nNOS) is an important therapeutic target for the treatment of various neurodegenerative disorders. A major challenge in the design of nNOS inhibitors focuses on potency in humans and selectivity over other NOS isoforms. Here we report potent and selective human nNOS inhibitors based on the 2-aminopyridine scaffold with a central pyridine linker. Compound **14j**, the most promising inhibitor in this study, exhibits excellent potency for rat nNOS (K_i 16 nM) with 828-fold n/e and 118-fold n/i, selectivity, with a K_i value of 13 nM against human nNOS with 1761-fold human n/e selectivity. Compound **14j** also displayed good metabolic stability in human liver microsomes, low plasma protein binding, and minimal binding to cytochromes P450 (CYPs), although it had little to no Caco-2 permeability.

Introduction

Nitric oxide (NO) is an essential second messenger in mammals,¹ which regulates a variety of biological processes, such as vasodilation,² smooth muscle relaxation,³ neurotransmission,⁴ and immune response.⁵ NO is generated by nitric oxide synthases (NOSs), of which there are three mammalian NOS isoforms: inducible NOS (iNOS), which activates the immune system to destroy pathogens and microorganisms;⁶ endothelial NOS (eNOS), which regulates the relaxation of smooth muscle, leading to a decrease of blood pressure;⁷ and neuronal NOS (nNOS), which regulates the release of neurotransmitters⁸ and is involved in neuronal communication.⁹ Overproduction of NO in the central nervous system (CNS) has been reported to be associated with chronic neurodegenerative pathogenesis,¹⁰ such as Alzheimer's disease (AD),¹¹ Parkinson's disease (PD),¹² and Huntington's disease (HD),¹³ as well as amyotrophic lateral sclerosis (ALS).¹⁴ Therefore, inhibition of nNOS is a viable therapeutic strategy for treating neurodegenerative disorders.

All of the mammalian NOSs are active only as homodimers,¹⁵ and each monomer consists of a C-terminal reductase domain, which contains the binding sites for NADPH (reduced nicotinamide adenine dinucleotide phosphate), FAD (flavin adenine dinucleotide), and FMN (flavin mononucleotide),¹⁶ and an N-terminal oxygenase domain, which contains binding sites for non-catalytic zinc (Zn^{2+}), catalytic heme, cofactor H₄B (tetrahydrobiopterin), and the substrate(L-Arg).¹⁷ NOSs catalyze the oxidation of L-Arg to L-citrulline and NO in the presence of oxygen and NADPH, and this cascade reaction is initiated by the two-electron donor NADPH in the reductase domain to the electron acceptor heme in the oxygenase domain through FAD and FMN with a series of proton transfers in the process.¹⁸

Given that all NOS isoforms catalyze the same reaction, the active site structures are nearly identical, which has made the development of isoform-selective inhibitors a challenging

1
2
3
4
5
6
7
8
9
10
11
12
13
14
15
16
17
18
19
20
21
22
23
24
25
26
27
28
29
30
31
32
33
34
35
36
37
38
39
40
41
42
43
44
45
46
47
48
49
50
51
52
53
54
55
56
57
58
59
60

problem. Nevertheless, it has been possible to exploit subtle difference in the active sites to develop highly selective nNOS inhibitors.¹⁹ Current efforts have been focused on improving bioavailability without sacrificing potency and selectivity. Various nNOS inhibitors that we have developed are shown in Figure 1. Thiophene-based inhibitors with diamine and hydroxyethyl-diamine structure (Figure 1, **1** and **2**, respectively)²⁰ show good potency against human nNOS. However, compound **2** gives very poor isoform selectivity over iNOS and eNOS ($n/I = 49$ and $n/e = 48$). Compound **3**,^{21,22} containing 2-aminopyridine, a pyrrolidine linker, and a diamine tail, is a moderate nNOS inhibitor ($K_i = 388$ nM) with good isoform selectivity (1114-fold over bovine eNOS and 150-fold over murine iNOS). Compound **4**,²³ a double-headed inhibitor, displays good potency against nNOS ($K_i = 25$ nM) but lacks good isoform selectivity ($n/e = 107$ and $n/i = 58$). Recently, our group reported a series of nNOS inhibitors with a 2-aminopyridine anchor, a heteroaromatic ring linker, and a diamine tail, such as compounds **5** and **6**.²⁴ Both display excellent potency for rat nNOS ($K_i = 17$ nM and 35 nM, respectively) and good selectivity over iNOS and eNOS (**5**: $n/i = 127$, $n/e = 759$; **6**: $n/i = 138$, $n/e = 507$). However, compounds **5** and **6** exhibit decreased potency against human nNOS (59 nM and 64 nM, respectively).

Although the human NOS isoforms are the ultimate target for these inhibitors, our efforts have focused on rat nNOS and bovine eNOS²⁵⁻³⁰ primarily because these two NOS isoforms generate the best crystals. However, we recently have been able to crystallize human nNOS and eNOS and have found that potencies for our inhibitors were generally 5-10 times less with human nNOS than with rat nNOS. This could be a problem for translation of preclinical animal studies to clinical trials, and could, in general, account for some drug failures in clinical trials. An overlay of human and rat nNOS crystal structures showed that the primary sequence in the active site and peripheral pocket of the rat enzyme is almost identical to that in the human enzyme except that Leu337 in the rat nNOS peripheral pocket is replaced by His342 in human nNOS. Consequently, the peripheral pocket of human nNOS tends to bind

1
2
3 smaller and more hydrophilic inhibitors, providing an insightful guide for the design of more
4
5 potent human nNOS inhibitors.^{24, 29b}
6

7
8 On the basis of reported NOS assay results and X-ray crystallographic analysis, we
9
10 performed specific and structure-based optimizations to improve the potency and selectivity
11
12 of lead **5**. Major modifications focused on exploring the diversity of the tail portion, leaving
13
14 the aminopyridine head and middle pyridine linker unmodified. First, we adopted a
15
16 ring-chain transformation strategy to give compound **14b**, based on the structure of **14a**, to
17
18 investigate the influence of a bulker and more hydrophobic tail on the potency and selectivity
19
20 of nNOS inhibitors. Second, an O atom and N atom were employed as bioisosteric
21
22 replacements in the piperidine ring of **14b** to make **14c** and **14g**, where the O atom or N atom
23
24 could possibly make a direct or indirect (water-assisted) H-bond network with the heme, H₄B,
25
26 or the surrounding residues within the active site of nNOS. Next, a ring-chain transformation
27
28 and homologation were used to design **14d** and **14e** from **14c**, and the piperazine tail of **14g**
29
30 was bioisosterically changed to a piperidine ring to obtain **14h**. Lastly, **14j** and **14k** were
31
32 synthesized, adopting a ring-chain transformation strategy from **14h** to investigate the
33
34 influence of flexibility on activity. The SAR of the secondary and tertiary amines on the tail
35
36 were explored to evaluate steric and polar effects.
37
38
39

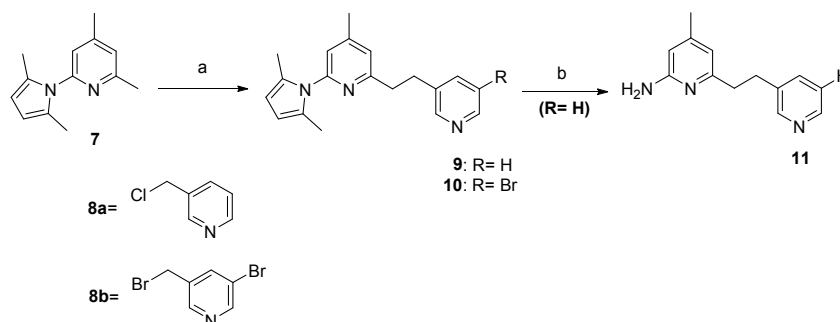
40
41 All compounds were assayed against purified rat nNOS, murine iNOS, and bovine eNOS
42
43 for preliminary evaluation of the potency and isoform selectivity for the NOSs in lower
44
45 animals. Many of the compounds were also assayed against human nNOS and eNOS to
46
47 determine human isoform selectivity.
48
49
50

51 CHEMISTRY

52
53 The synthesis of compounds **10** and **11** is shown in Scheme 1. Compound **11** was
54
55 prepared in two steps, coupling 3-chloromethylpyridine (**8a**) with lithiated
56
57 pyrrolyl-4,6-dimethylpyridine (**7**) followed by pyrrole deprotection.²⁴ Intermediate **10** was
58
59
60

synthesized by the same coupling reaction described above using aryl bromide **8b**.

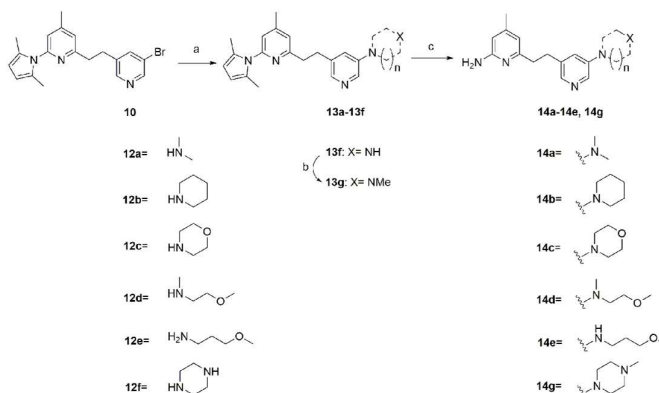
Scheme 1. Synthesis of intermediate **10** and compound **11**



Reagents and conditions (a) **8a** or **8b**, *n*-BuLi, THF, -78 °C to 0 °C then -78 °C; (b) NH₂OH·HCl, EtOH/H₂O (2:1), 100 °C, 20 h.

As shown in Scheme 2, compounds **14a-14e** were synthesized by palladium-catalyzed Buchwald-Hartwig amination of intermediate **10** with amines **12a-12e**^{24,31} followed by pyrrole deprotection.²⁴ Compound **10** was subjected to palladium-catalyzed amination with **12f** to give **13f**, which was methylated (**13g**), and the pyrrole was deprotected to afford **14g**.

Scheme 2. Synthesis of compounds **14a-14e** and **14g**

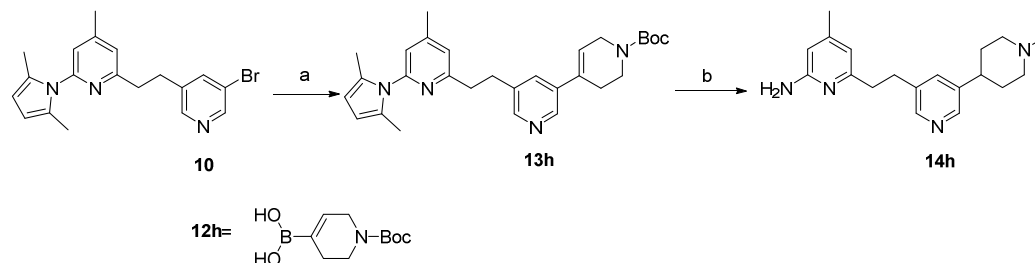


Reagents and conditions: (a) **12a**, **12b**, **12c**, **12d**, **12e**, or **12f**, Pd₂(dba)₃, DavePhos, NaO*t*-Bu, dioxane, 100 °C, 20 h; (b) MeI, TEA, THF, r.t., 1 h; (c) NH₂OH·HCl, EtOH/H₂O (2:1), 100

°C, 20 h.

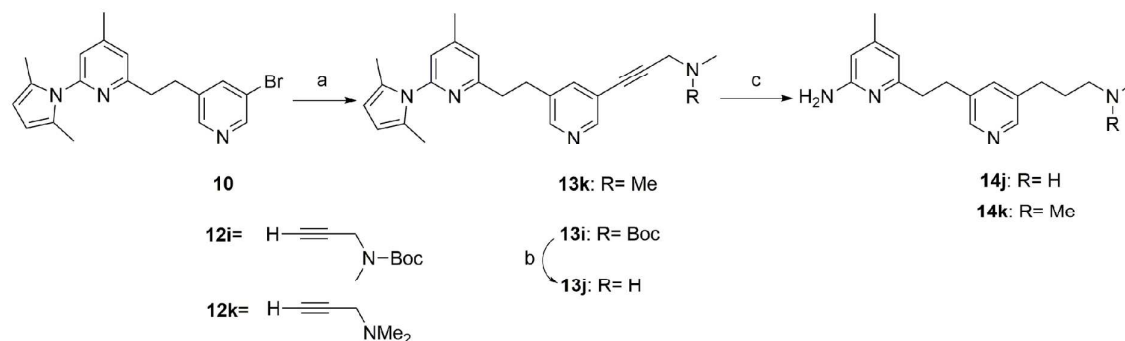
The synthesis of **14h** is shown in Scheme 3. Compound **13h** was obtained via Suzuki cross-coupling³² employing **10** and boronic acid **12h**; **13h** subsequently underwent alkene reduction, carbamate reduction, and pyrrole deprotection to give **14h**. Compound **14j** and **14k** were synthesized according to Scheme 4. Compound **14j** was prepared in three steps including a Sonagashira cross-coupling³³ of **10** with *N*-Boc-*N*-methyl-propargylamine (**12i**), Boc deprotection, and pyrrole deprotection. Sonagashira cross-coupling of **10** with 3-dimethylamino-1-propyne (**12k**) followed by pyrrole deprotection gave **14k**.

Scheme 3. Synthesis of 14h



Reagents and conditions (a) **12h**, Pd(OAc)₂, SPhos, K₃PO₄, Tol/H₂O (20:1), 100 °C, 20 h; (b) (i) Pd/C, H₂, MeOH, r.t., 20 h, (ii) LAH, THF, 0 °C to reflux, 1 h, (iii) NH₂OH·HCl, EtOH/H₂O (2:1), 100 °C, 20 h.

Scheme 4. Synthesis of compounds 14j and 14k



1
2
3
4
5
6 Reagents and conditions: (a) **12i** or **12k**, Pd(PPh₃)₄, CuI, TEA, 90 °C, 20 h; (b) 20 % TFA in
7
8 DCM, r.t., 1 h; (c) (i) Pd/C, H₂, MeOH, r.t., 20 h, (ii) NH₂OH·HCl, EtOH/H₂O (2:1), 100 °C,
9
10 20 h.

11 12 13 14 RESULTS AND DISCUSSION

15 16 Inhibition of nonhuman NOSs

17
18 Synthesized inhibitors were assayed against purified rat nNOS, murine macrophage iNOS,
19
20 bovine eNOS, and human nNOS and eNOS using the hemoglobin capture assay.^{34,35} The *K_i*
21
22 values and isoform selectivities for inhibitors **11**, **14a-14e**, **14g**, **14h**, **14j**, and **14k** against
23
24 nonhuman NOSs are shown in Table 1; values for **4**,²³ **5**,²⁴ and **6**²⁴ are included for
25
26 comparison. The excision of the terminal pyridino or amino group from **4-6** is highly
27
28 detrimental to the potency (see **11-14e**). Addition of a second amino group by attachment of a
29
30 piperazine (**14g**) or piperidine (**14h**) ring begins to restore the excellent potencies and
31
32 selectivities of **4-6**. The crystal structures of nNOS-**14g** (Figure 4A) and nNOS-**5** (Figure 4C)
33
34 reveal a similar and unique inhibitor binding mode. In addition to the
35
36 2-aminopyridine-Glu592 H-bond, the pyridine linker bends upward forming a H-bond to
37
38 Tyr562 (3.0 Å). To allow this upward pyridine position the Gln478 side chain has to adapt to
39
40 an alternate rotamer form. The external N atom in the piperazine ring joins a H-bonding
41
42 network involving H₄B and heme propionate A *via* a water molecule (external N to water: 3.0
43
44 Å; water to H₄B: 2.7 Å; water to heme propionate A: 2.6 Å). In contrast, for **5**, although the
45
46 internal N atom position in the tail is well-defined, the positions of the last three atoms are
47
48 ambiguous, having weaker density.²⁴

49
50 The internal N atom in the tail region attached to the pyridine linker does not interact with
51
52 the surrounding residues, as shown in both the nNOS-**14g** and nNOS-**5** complexes. On the
53
54 basis of the crystal structures, **14h** was synthesized as a bioisostere of **14g** without the
55
56
57
58
59
60

1
2
3
4 internal N atom in the piperazine ring. As shown in the crystal structure of nNOS-**14h** (Figure
5
6 4B), in addition to the strong 2-aminopyridine-Glu592 salt bridge, the N atom in the pyridine
7
8 linker forms a H-bond to Tyr562 (3.0 Å), and the N atom in the piperazine ring also
9
10 participates in a water-assisted H-bonding network with the H₄B and heme propionate A (N
11
12 atom to water: 2.9 Å; water to H₄B: 2.6 Å; water to heme propionate A: 2.7 Å). Therefore,
13
14 **14g**, **14h**, and **5** bind identically to rat nNOS with the pyridine linker in an upward position,
15
16 i.e., in which the pyridine N faces away from the heme. The differences in potency among
17
18 **14g**, **14h**, and **5** could be explained by the flexibility of the tail region and the strength
19
20 (H-bond distance) of the interaction made by the central pyridine linker to Tyr562.

21
22
23 Compound **14g** is a very weak inhibitor of bovine eNOS ($K_i > 30000$ nM), at least 2.5-fold
24
25 less potent than reference compound **5** (K_i 12910 nM); consequently, it is highly selective for
26
27 nNOS over eNOS (n/e > 698). The crystal structure of eNOS-**14g** (Figure 6A) shows that
28
29 while the 2-aminopyridine forms H-bonds with Glu363, the pyridine linker is no longer in the
30
31 upward position. Rather, it forms a H-bonding network involving the H₄B and heme
32
33 propionate A *via* a water molecule (N atom to water: 2.7 Å; water to H₄B: 2.6 Å; water to
34
35 heme propionate A: 2.5 Å), and the external N atom in the piperazine ring forms a weak
36
37 H-bond with Asn340 (3.4 Å). In comparison, the central pyridine linker in the eNOS-**5**
38
39 complex (Figure 6B) is also in a flat binding mode, and the tail region of **5** does not interact
40
41 with the enzyme. The pyridine linker in **14g** is parallel to the 2-aminopyridine anchor, while
42
43 the pyridine linker in **5** makes a 15° angle from the 2-aminopyridine plane, which does not
44
45 involve the H-bonding network with H₄B and heme. The excellent n/e selectivities for **14g**
46
47 and **5** are very likely the result of the drastically different pyridine linker positions in the two
48
49 isoforms.
50
51
52

53
54 The most potent and selective analogues (**14j** and **14k**) have flexible side chains
55
56 resembling that in **5**, except that the *N*-methylamino group adjacent to the pyridine ring has
57
58 been replaced by a methylene group. In a comparison of the crystal structures of nNOS-**14j**
59
60

1
2
3 and nNOS-**14k** (Figure 6) with that of nNOS-**5** (Figure 4C), the 2-aminopyridine-Glu592
4 interaction and the identical upward pyridine linker binding mode are observed in all three of
5
6 the complexes. In the nNOS-**14j** complex, the secondary amine N atom in the tail region
7
8 joins a water-assisted H-bonding network with the H₄B and heme propionate A (N atom to
9
10 water: 2.9 Å; water to H₄B: 2.6 Å; water to heme propionate A: 2.6 Å). In the **14k**-nNOS
11
12 complex, the tertiary amine N atom in the tail region also participates in a water-bridged
13
14 H-bonding network involving the H₄B and heme propionate A (N atom to water: 2.6 Å; water
15
16 to H₄B: 2.6 Å; water to heme propionate A: 2.6 Å). The involvement of the inhibitor tail
17
18 region with a H-bonding network seems to improve potency.
19
20
21
22

23 Consistent with the observed high n/e selectivity, the crystal structure of eNOS-**14k**
24 (Figure 6C) shows that the upward pyridine linker binding mode of **14k** in nNOS is not
25
26 observed in eNOS. Rather, its linker pyridine is parallel to the plane of the aminopyridine
27
28 anchor, making H-bonds with Asn368 *via* a bridging water molecule (N atom to water: 2.9 Å;
29
30 water to Asn368: 2.9 Å). In addition, the tertiary amine N on the tail forms a H-bond with
31
32 heme propionate D (2.9 Å).
33
34
35
36
37

38 Inhibition of human NOSs

39
40 The primary sequence of human and rat NOS is more than 93% identical,²⁴ and the nNOS
41
42 active site in each mammalian isozyme is highly conserved. The peripheral pockets of
43
44 human- and rat nNOS differ by only one residue (His342 in human and Leu337 in rat).^{24,36} If
45
46 the inhibitor is designed so it is too small to reach the His342/Leu337 site, an identical
47
48 binding mode should be observed in both the human and rat nNOS-inhibitor complexes,²⁴ and
49
50 the difference in potency of an inhibitor for the enzyme in these species should be
51
52 insignificant (K_i human nNOS /rat nNOS close to 1). Compounds **5** and **6** fit into this
53
54 classification, and the human nNOS/rat nNOS ratios for these compounds were 3.5 and 1.8,
55
56 respectively.
57
58
59
60

1
2
3
4
5
6
7
8
9
10
11
12
13
14
15
16
17
18
19
20
21
22
23
24
25
26
27
28
29
30
31
32
33
34
35
36
37
38
39
40
41
42
43
44
45
46
47
48
49
50
51
52
53
54
55
56
57
58
59
60

Compounds **14a**, **14c**, **14g**, **14h**, **14j**, and **14k**, which also have truncated side-chains, were assayed against purified human nNOS (Table 2). Four of these analogues, **14c**, **14h**, **14j**, **14k**, had human nNOS/rat nNOS ratios lower than 1.8; **14j** is the first potent compound with a human nNOS/rat nNOS ratio < 1. The benefit of a human/rat K_i ratio of 1 or less is that results in a preclinical rodent model might translate to humans in clinical trials.

As shown in Figure 7A, the 2-aminopyridine group of **14g** forms H-bonds with Glu597 in human nNOS (Glu592 in rat); the N atom in the pyridine linker makes a H-bond with Tyr567 (2.8 Å) (Tyr562 in rat); the external N atom in the piperazine ring joins a H-bond network involving H₄B and heme propionate A *via* a water molecule (external N to water: 2.9 Å; water to H₄B: 3.0 Å; water to heme propionate A: 2.5 Å). In the human nNOS-**14h** complex (Figure 7B), the same H-bonds exist between the 2-aminopyridine group of **14h** and Glu597; the N atom of the pyridine linker makes a H-bond to Tyr567 (3.0 Å), and the external N atom in the piperazine ring participates in a water-assisted H-bonding network involving H₄B and heme propionate A (external N to water: 2.7 Å; water to H₄B: 2.8 Å; water to heme propionate A: 2.7 Å).

The human nNOS-**14g** crystal structure (Figure 7A) shows an identical upward pyridine linker binding mode as shown in Figure 4A (rat nNOS-**14g**) because **14g** is too short to reach the His342/Leu337 site (His342 is at least 8 Å away from **14g**). Similarly, an identical binding mode is observed in both human and rat nNOS-**14h** complexes (Figure 7B and Figure 4B).

Compound **14j** is comparable in potency and selectivity to those of compound **5**; **14k** has two-thirds the potency of **5** with lower selectivity. Crystal structures of these compounds bound to human nNOS show that **14j** (Figure 8A) H-bonds to Glu597 through the 2-aminopyridine group; the N atom in the pyridine linker forms two H-bonds to Tyr567 (2.8 Å) and Tyr593 (3.4 Å) (Tyr588 in rat), and the N atom in the tail region participates in a tight H-bonding network involving the H₄B and heme propionate A through a water molecule (N

1
2
3 to water: 2.6 Å; water to H₄B: 2.8 Å; water to heme propionate A: 2.6 Å). Similar interactions
4 are involved in the **14k** complex (Figure 8B). In addition to the 2-aminopyridine-Glu597
5 interaction, the N atom in the pyridine linker forms two H-bonds to Tyr567 (2.8 Å) and
6 Tyr593 (3.5 Å), and the N atom in the tail region joins a water-mediated H-bond network
7 with H₄B and heme propionate A (N to water: 2.5 Å; water to H₄B: 2.9 Å; water to heme
8 propionate A: 2.7 Å). The structures of human nNOS-**14j** and -**14k** reveal a subtle but
9 important feature: the N atom in the pyridine linker is involved in two H-bonds; the distance
10 to Tyr593 is within 3.5 Å. This is the consequence of a long tail region where its amine N
11 atom is part of a tight H-bonding network with the H₄B and heme *via* a water molecule. The
12 network pushes the pyridine linker closer to Tyr567 and Tyr593. This feature does not exist in
13 structures of human nNOS-**14g** or -**14h** because the H-bonding network there is established
14 by shorter piperidine or piperazine moieties. In all of the rat nNOS structures in complex with
15 **14g**, **14h**, **14j**, and **14k**, the N atom in the pyridine linker is also only making one H-bond
16 with Tyr562, but not with Tyr588. A comparison with the binding interactions in human
17 nNOS-**5** (Figure 8C) is interesting as well. While the 2-aminopyridine group in **5** is also
18 anchored by Glu597, the N atom of the central pyridine ring makes only one hydrogen bond,
19 that is, with Tyr567, and the external N atom in the tail region displaces the bridging water
20 molecule between the H₄B and heme propionate A.²⁴ All three inhibitors, **14j**, **14k**, and **5**,
21 exhibit the same upward pyridine binding mode in human nNOS; the differences in the
22 enzyme-inhibitor interactions, especially in the number and distances of the H bonds, appear
23 to account for the compound potency differences.

24
25
26
27
28
29
30
31
32
33
34
35
36
37
38
39
40
41
42
43
44
45
46
47
48
49 An alignment of human nNOS and eNOS reveals four important residue differences:
50 Ser607/His371, His342/Phe305, Met341/Val104, and Asp602/Asn366. Among these four
51 amino acid pairs, the Asp602/Asn366 difference in human nNOS/eNOS makes the nNOS
52 active site more electronegative than eNOS, and this electronic difference can be used for
53 selective inhibition (nNOS tends to bind positively charged compounds).
54
55
56
57
58
59
60

1
2
3
4
5
6
7
8
9
10
11
12
13
14
15
16
17
18
19
20
21
22
23
24
25
26
27
28
29
30
31
32
33
34
35
36
37
38
39
40
41
42
43
44
45
46
47
48
49
50
51
52
53
54
55
56
57
58
59
60

Compounds **14a**, **14c**, **14g**, **14h**, **14j**, and **14k** were assayed against purified human eNOS and compared with **5** and **6** (Table 3). Once again, **14j** exhibited the best selectivity properties of these compounds, 1761-fold more potent against human nNOS than human eNOS. Although **14g** had the least affinity for human eNOS, its potency with human nNOS was 6.5 times worse than that for **14j**, so the selectivity of **14g** was about half that of **14j**.

Effect of **14j** on CYPs

The two pyridines in **14j** make it a potential inhibitor of cytochromes P450 (CYPs). Consequently, **14j** was evaluated for its inhibition of seven major human liver microsomal P450s (Table 4). At a concentration 769 times its K_i against human nNOS (10 μM), it was found to inhibit the activity of CYP1A2, CYP2B6, CYP2C8, CYP2C9, CYP2C19, and CYP2D6 insignificantly; the only isozyme that showed any significant inhibition was CYP3A4 (58%). The IC_{50} of compound **14j** for CYP3A4 is estimated to be approximately 10 μM , and the selectivity toward nNOS is more than 70-fold in rat (IC_{50} 0.142 μM) and 100-fold in human (IC_{50} 0.091 μM). Therefore, the inhibitory potency of **14j** for CYP3A4 is relatively weak.

Other pharmacokinetic properties of **14j**

Other pharmacokinetic properties that were tested with **14j** included human microsome stability and plasma protein binding. At 1 μM concentration, the half-life of **14j** in human liver microsomes was > 60 min; however, the metabolism was unrelated to CYP-mediated metabolism, as 23% of the compound was lost in 60 min in the absence of NADPH or in 90 min in the presence of NADPH. At 5 μM concentration, only 20% bound to human plasma protein. Unfortunately, **14j** exhibited little or no Caco-2 permeability. Detailed experimental results and protocol can be found in the Supporting Information.

CONCLUSIONS

A series of human nNOS inhibitors, based on the 2-aminopyridine scaffold having a central pyridine linker, were designed and evaluated. Compound **14j** had outstanding properties, exhibiting a potent and slightly lower K_i value for human nNOS (13 nM) than rat nNOS (16 nM) with 118-fold and 1761-fold selectivity over mouse iNOS and human eNOS, respectively. X-ray crystal structures of **14j** bound to both rat and human nNOS showed that the N of the pyridine linker formed two H-bonds (to Tyr567 and Tyr593) in human nNOS but only one H-bond in rat nNOS. Compound **14j** displayed very poor inhibition of human CYPs (except 58% inhibition of CYP3A4 at 10 μ M), little or no human microsome CYP metabolism for at least 60 min, and only 20% human plasma protein binding. However, it had little or no Caco-2 permeability, predicting that oral absorption would be poor.

EXPERIMENTAL SECTION

Materials, Synthetic Methods, and Characterization of Molecules. Commercially available starting materials **12a-12f** were purchased from Sigma-Aldrich and were used without further purification. All reactions were performed under an atmosphere of dry argon. Compounds **7**, **8a**, **8b**, **12h**, and **12i** were prepared by known literature procedures using commercially available chemicals (**7-s**, **8a-S**, **8b-S**, **12h-S**, and **12i-S**; see Supporting Information for details), and their spectral data are consistent with those data reported for them.

Anhydrous solvents (CH_2Cl_2 and THF) were purified prior to use by passage through a column composed of activated alumina and a supported copper redox catalyst. Analytical thin-layer chromatography was carried out on SiliCycle pre-coated silica gel 60 F254 plates. Compounds were visualized with short-wavelength UV light, ninhydrin, or KMnO_4 stain. Flash column chromatography was performed using an Agilent 971-FP automated flash purification system with a Varian column station and various SiliCycle cartridges (4–80 g,

1
2
3 40-63 μm , 60 \AA). ^1H NMR and ^{13}C NMR spectra were recorded in the indicated solvent on a
4
5 Bruker Avance-III (500 MHz and 125 MHz for ^1H and ^{13}C , respectively) spectrometer.
6
7 Low-resolution ESIMS was performed using a Bruker AmaZon SL Ion Trap mass
8 spectrometer system. High-resolution mass spectra were obtained using an Agilent 6210
9
10 LC-TOF spectrometer in the positive ion mode using electrospray ionization with an Agilent
11
12 G1312A HPLC pump and an Agilent G1367B auto injector at the Integrated Molecular
13
14 Structure Education and Research Center (IMSERC), Northwestern University. The purity of
15
16 the compounds was evaluated on an analytical HPLC. Analytical HPLC was performed using
17
18 an Agilent Infinity 1260 HPLC system with a Phenomenex Luna C-8 (4.6 \times 250 mm, 5 μm)
19
20 reverse phase column, detecting with UV absorbance (254 nm). The purity of all compounds
21
22 that were subjected to biological assay was > 95%.
23
24
25
26

27 **General Procedure A: Pyrrolyl-lutidine and Aryl Halide Coupling.** A round bottom
28 flask was charged with **7** (1 equiv.), and THF was added to form a 0.2 M solution. *n*-BuLi
29 (1.6 equiv.) was added to the solution at -78 $^\circ\text{C}$, and the reaction mixture was allowed to stir
30 for 30 min at 0 $^\circ\text{C}$. The mixture was transferred to a 1 M solution of aryl halide (**8a** or **8b**) in
31 THF *via* cannula at -78 $^\circ\text{C}$, which was allowed to stir for an additional 20 min then quenched
32 with H_2O . The crude reaction mixture was partitioned between ethyl acetate and water, and
33 the organic layer was washed with H_2O and brine, dried with Na_2SO_4 , and concentrated under
34 reduced pressure. The crude product was purified by flash column chromatography to give **9**
35 and **10**.
36
37
38
39
40
41
42
43
44
45

46
47 **2-(2,5-Dimethyl-1*H*-pyrrol-1-yl)-4-methyl-6-(2-(pyridin-3-yl)ethyl)pyridine (9).**

48
49 Compound **9** was synthesized according to general procedure **A** using **7** (600 mg, 3 mmol)
50 and **8a** (681 mg, 3 mmol). **9** was isolated as a yellow oil (343 mg, 39%) after flash column
51 chromatography (ethyl acetate: hexanes 1:1). ^1H NMR (500 MHz, CDCl_3): δ 8.41-8.39 (m,
52 2H), 7.46 (d, J = 5.0 Hz, 1H), 7.16 (dd, J = 7.0, 5.0 Hz, 1H), 6.87 (s, 1H), 6.84 (s, 1H), 5.86
53 (s, 2H), 3.06-3.05 (m, 4H), 2.33 (s, 3H), 2.09 (s, 6H); ^{13}C NMR (125 MHz, CDCl_3): δ 160.1,
54
55
56
57
58
59
60

1
2
3 151.8, 150.0, 149.6, 147.5, 136.7, 135.9, 128.5, 123.3, 122.7, 120.3, 106.8, 39.1, 32.7, 21.0,
4
5 13.2; MS ESI: calcd. For C₁₉H₂₂N₃ [M+H]⁺, 292.18; found, 292.08.

7
8 **2-(2-(5-Bromopyridin-3-yl)ethyl)-6-(2,5-dimethyl-1H-pyrrol-1-yl)-4-methylpyridine**

9
10 **(10)**. Compound **10** was synthesized according to general procedure **A** using **7** (400 mg, 2
11 mmol) and **8b** (500 mg, 2 mmol). **10** was isolated as a yellow oil (273.2 mg, 46%) after flash
12 column chromatography (ethyl acetate: hexanes 1:4). ¹H NMR (500 MHz, CDCl₃): δ 8.48 (s,
13 1H), 8.30 (s, 1H), 7.60 (s, 1H), 6.87 (s, 1H), 6.86 (s, 1H), 5.87 (s, 2H), 3.06-3.05 (m, 4H),
14 2.35 (s, 3H), 2.09 (s, 6H); ¹³C NMR (125 MHz, CDCl₃): δ 159.4, 151.9, 149.8, 148.2, 147.6,
15 139.1, 138.9, 128.5, 122.8, 120.6, 120.5, 106.8, 38.7, 32.1, 21.0, 13.2; MS ESI: calcd. For
16 C₁₉H₂₁BrN₃ [M+H]⁺, 372.09; found, 372.05.

17
18
19
20
21
22
23
24
25 **4-Methyl-6-(2-(pyridin-3-yl)ethyl)pyridin-2-amine (11)**. **11** was synthesized according
26 to general procedure **D** using **9** (48.0 mg) and NH₂OH·HCl (46.9 mg). **11** was isolated as a
27 brown oil (33.5 mg, 95%) after flash column chromatography (MeOH: DCM 3:7). ¹H NMR
28 (500 MHz, Methanol-*d*₄): δ 8.93 (s, 1H), 8.80 (d, *J* = 6.0 Hz, 1H), 8.66 (d, *J* = 8.0 Hz, 1H),
29 8.09 (dd, *J* = 8.0, 6.0 Hz, 1H), 6.72 (s, 1H), 6.70 (s, 1H), 3.36-3.33 (m, 2H), 3.18-3.15 (m,
30 2H), 2.37 (s, 3H); ¹³C NMR (125 MHz, methanol-*d*₄): δ 157.7, 154.6, 147.0, 146.9, 141.2,
31 140.7, 139.7, 127.2, 113.7, 110.0, 32.6, 31.0, 20.6; HRMS ESI: calcd. For C₁₃H₁₆N₃ [M+H]⁺,
32 214.1339; found, 214.1337.

33
34
35
36
37
38
39
40
41
42 **General Procedure B: Preparation of 13a-13e and 13g (Buchwald-Hartwig**
43 **Palladium-Catalyzed Amination of 10)**. A microwave vial was charged with Pd₂(dba)₃(5
44 mol%), Davephos (10 mol%), NaO^tBu (1.2 equiv.), **10** (1 equiv.) and amine **12a-12f** (1.5-2
45 equiv.). The mixtures were diluted with dioxane to form a 0.16 M solution. The microwave
46 vial was then capped, and the reaction mixture was stirred at 100 °C for 20 h. At this time, the
47 cap was removed, and the reaction mixture was filtered through a silica pad. The filtrate was
48 concentrated under reduced pressure and purified by flash column chromatography to give
49 **13a-13e** and **13g**.

1
2
3
4
5
6
7
8
9
10
11
12
13
14
15
16
17
18
19
20
21
22
23
24
25
26
27
28
29
30
31
32
33
34
35
36
37
38
39
40
41
42
43
44
45
46
47
48
49
50
51
52
53
54
55
56
57
58
59
60

5-(2-(6-(2,5-Dimethyl-1*H*-pyrrol-1-yl)-4-methylpyridin-2-yl)ethyl)-*N,N*-dimethylpyridin-3-amine (13a). Compound **13a** was synthesized according to general procedure **B** using Pd₂(dba)₃ (12.1 mg), Davephos (10.2 mg), NaO^tBu (29.2 mg), **10** (93.3 mg), and amine **12a** (0.25 ml, 2M in THF). **13a** was isolated as a yellow oil (42.3 mg, 50%) after flash column chromatography (MeOH: DCM 1:19). ¹H NMR (500 MHz, CDCl₃): δ 7.95 (s, 1H), 7.79 (s, 1H), 6.90 (s, 1H), 6.84 (s, 1H), 6.77 (s, 1H), 5.86 (s, 2H), 3.07-3.03 (m, 2H), 3.02-2.98 (m, 2H), 2.91 (s, 6H), 2.34 (s, 3H), 2.10 (s, 6H); ¹³C NMR (125 MHz, CDCl₃): δ 160.4, 151.7, 149.6, 146.1, 137.6, 136.7, 132.6, 128.5, 122.7, 120.2, 119.2, 106.8, 40.1, 39.4, 33.1, 21.0, 13.2.

2-(2,5-Dimethyl-1*H*-pyrrol-1-yl)-4-methyl-6-(2-(5-(piperidin-1-yl)pyridin-3-yl)ethyl)pyridine (13b). Compound **13b** was synthesized according to general procedure **B** using Pd₂(dba)₃ (13.2 mg), Davephos (10.8 mg), NaO^tBu (32.1 mg), **10** (102 mg, 0.28 mmol), and amine **12b** (46.8 mg, 0.55 mmol). **13b** was isolated as a yellow oil (73.2 mg, 71%) after flash column chromatography (ethyl acetate: hexanes 8:1). ¹H NMR (500 MHz, CDCl₃): δ 8.10 (s, 1H), 7.85 (s, 1H), 6.97 (s, 1H), 6.87 (s, 1H), 6.84 (s, 1H), 5.86 (s, 2H), 3.12 (t, *J* = 5.0 Hz, 4H), 3.06-2.98 (m, 4H), 2.34 (s, 3H), 2.10 (s, 6H), 1.68-1.64 (m, 4H), 1.59-1.54 (m, 2H); ¹³C NMR (125 MHz, CDCl₃): δ 160.3, 151.8, 149.6, 147.6, 139.4, 136.9, 136.0, 128.4, 123.2, 122.8, 120.2, 106.8, 49.8, 39.3, 32.9, 25.5, 24.1, 21.0, 13.3.

4-(5-(2-(6-(2,5-Dimethyl-1*H*-pyrrol-1-yl)-4-methylpyridin-2-yl)ethyl)pyridin-3-yl)morpholine (13c). Compound **13c** was synthesized according to general procedure **B** using Pd₂(dba)₃ (11.4 mg), Davephos (9.6 mg), NaO^tBu (28.2 mg), **10** (88.1 mg), and amine **12c** (44.2 mg). **13c** was isolated as a yellow oil (86.6 mg, 96%) after flash column chromatography (MeOH: DCM 1:19). ¹H NMR (500 MHz, CDCl₃): δ 8.07 (s, 1H), 7.92 (s, 1H), 6.96 (s, 1H), 6.88 (s, 1H), 6.84 (s, 1H), 5.87 (s, 2H), 3.82 (t, *J* = 5.0 Hz, 4H), 3.11 (t, *J* = 5.0 Hz, 4H), 3.08-3.06 (m, 4H), 2.35 (s, 3H), 2.09 (s, 6H); ¹³C NMR (125 MHz, CDCl₃): δ 160.2, 151.7, 149.6, 146.7, 141.2, 136.8, 136.0, 128.4, 122.7, 122.4, 120.2, 106.8, 66.7, 48.6,

39.2, 32.8, 21.0, 13.3; MS ESI: calcd. For C₂₃H₂₉N₄O [M+H]⁺, 377.23; found, 377.18.

5-(2-(6-(2,5-Dimethyl-1*H*-pyrrol-1-yl)-4-methylpyridin-2-yl)ethyl)-*N*-(2-methoxyethyl)-*N*-methylpyridin-3-amine (13d). Compound **13d** was synthesized according to general procedure **B** using Pd₂(dba)₃ (12.0 mg), Davephos (10.1 mg), NaO^tBu (29.4 mg), **10** (93.5 mg, 0.25 mmol), and amine **12d** (46.1 mg). **13d** was isolated as a yellow oil (61.8 mg, 65%) after flash column chromatography (MeOH: DCM 1:19). ¹H NMR (500 MHz, CDCl₃): δ 7.95 (s, 1H), 7.70 (s, 1H), 6.90 (s, 1H), 6.84 (s, 1H), 6.77 (s, 1H), 5.86 (s, 2H), 3.52-3.50 (m, 2H), 3.47-3.45 (m, 2H), 3.32 (s, 3H), 3.07-3.03 (m, 2H), 3.00-2.97 (m, 2H), 2.93 (s, 3H), 2.34 (s, 3H), 2.10 (s, 6H); ¹³C NMR (125 MHz, CDCl₃): δ 160.5, 151.7, 149.6, 145.0, 137.7, 136.7, 132.6, 128.4, 122.7, 120.2, 118.7, 106.8, 70.1, 59.1, 52.1, 39.4, 38.6, 33.1, 21.0, 13.2.

5-(2-(6-(2,5-Dimethyl-1*H*-pyrrol-1-yl)-4-methylpyridin-2-yl)ethyl)-*N*-(3-methoxypropyl)pyridin-3-amine (13e). Compound **13e** was synthesized according to general procedure **B** using Pd₂(dba)₃ (12.0 mg), Davephos (10.2 mg), NaO^tBu (29.5 mg), **10** (94 mg), and amine **12e** (46.3 mg). **13e** was isolated as a yellow oil (66.5 mg, 70%) after flash column chromatography (MeOH: DCM 1:19). ¹H NMR (500 MHz, CDCl₃): δ 7.82 (s, 1H), 7.73 (s, 1H), 6.89 (s, 1H), 6.83 (s, 1H), 6.66 (s, 1H), 5.85 (s, 2H), 4.06 (brs, 1H), 3.47 (t, *J* = 6.0 Hz, 2H), 3.32 (s, 3H), 3.16 (t, *J* = 6.5 Hz, 2H), 3.04-3.01 (m, 2H), 2.96-2.93 (m, 2H), 2.33 (s, 3H), 2.09 (s, 6H), 1.86-1.81 (m, 2H); ¹³C NMR (125 MHz, CDCl₃): δ 160.5, 151.7, 149.6, 149.5, 138.5, 134.0, 133.9, 128.4, 122.7, 120.2, 118.5, 106.7, 71.2, 58.8, 41.6, 39.3, 32.9, 29.2, 21.0, 13.2; MS ESI: calcd. For C₂₃H₂₉N₄O [M+H]⁺, 379.25; found, 379.20.

1-(5-(2-(6-(2,5-Dimethyl-1*H*-pyrrol-1-yl)-4-methylpyridin-2-yl)ethyl)pyridin-3-yl)-4-methylpiperazine (13g). Compound **13g** was synthesized by methylation of **13f**. Compound **13f** was prepared according to general procedure **B** using Pd₂(dba)₃ (28.1 mg), Davephos (24.1 mg), NaO^tBu (70.7 mg), **10** (226.2 mg), and piperazine **12f** (105.4 mg). Crude product **13f** was subjected to methylation without purification. A scintillation vial was charged with **13f** (1 equiv.). The crude product was diluted with THF to form a 0.1 M solution followed by

1
2
3 addition of triethylamine (1.5 equiv.) and MeI (1 equiv.). The reaction mixture was allowed to
4 stir at r.t. for 1 h. The crude product was diluted with DCM and washed with water and brine.
5
6 The organic layer was dried with Na₂SO₄ and concentrated under reduced pressure. The crude
7
8 product mixture was purified by flash column chromatography (MeOH: DCM 1:6) to give
9
10 **13g** (34.6 mg, 15% for the two steps). ¹H NMR (500 MHz, CDCl₃): δ 8.09 (s, 1H), 7.89 (s,
11 1H), 6.97 (s, 1H), 6.87 (s, 1H), 6.83 (s, 1H), 5.84 (s, 2H), 3.20 (t, *J* = 5.0 Hz, 4H), 3.04-2.99
12 (m, 4H), 2.60 (t, *J* = 5.0 Hz, 4H), 2.36 (s, 3H), 2.33 (s, 3H), 2.08 (s, 6H); ¹³C NMR (125
13 MHz, CDCl₃): δ 160.2, 151.7, 149.6, 146.6, 140.9, 136.8, 136.3, 128.4, 122.8, 122.7, 120.3,
14 106.8, 54.7, 48.1, 45.9, 39.2, 32.9, 21.0, 13.2.

15
16
17
18
19
20
21
22
23 ***tert*-Butyl-4-(5-(2-(6-(2,5-dimethyl-1*H*-pyrrol-1-yl)-4-methylpyridin-2-yl)ethyl)pyridi-**
24
25 ***n*-3-yl)-5,6-dihydropyridine-1(2*H*)-carboxylate (13h).** A microwave vial was charged with
26 Pd(OAc)₂ (13.4 mg), SPhos (41.1 mg), K₃PO₄ (849.1 mg), boronic acid **12f** (459.2 mg), and
27 **10** (364 mg, 1.0 mmol). The mixture was diluted with toluene/water (20:1) to form a 0.13 M
28 solution. The microwave vial was capped, and the reaction mixture was stirred at 100 °C for
29 20 h. The cap was removed, and the reaction mixture was diluted with ethyl acetate. The
30 crude product was filtered, the filtrate was dried over Na₂SO₄, and concentrated under
31 reduced pressure. **13h** was isolated as a yellow oil (316.2 mg, 68%) after flash column
32 chromatography (ethyl acetate: hexanes 1:1). ¹H NMR (500 MHz, CDCl₃): δ 8.43 (s, 1H),
33 8.27 (s, 1H), 7.44 (s, 1H), 6.87 (s, 1H), 6.84 (s, 1H), 6.02-6.01 (m, 1H), 5.86 (s, 2H),
34 4.07-4.05 (m, 2H), 3.62-3.60 (m, 2H), 3.08-3.07 (m, 4H), 2.45-2.43 (m, 2H), 2.34 (s, 3H),
35 2.08 (s, 6H), 1.47 (s, 9H); ¹³C NMR (125 MHz, CDCl₃): δ 159.9, 154.8, 151.8, 149.7, 148.3,
36 148.2, 144.1, 136.4, 135.8, 132.7, 132.6, 128.4, 122.7, 120.3, 106.8, 79.9, 39.1, 39.0, 32.6,
37 32.5, 28.5, 27.1, 21.0, 13.2.

38
39
40
41
42
43
44
45
46
47
48
49
50
51
52
53
54 **General Procedure C: Preparation of 13i and 13k (Sonagashira-Cross Coupling of**
55 **10).** A microwave vial was charged with Pd(PPh₃)₄ (5 mol%), CuI (5 mol%), and **10** (1
56 equiv.). The mixtures were diluted with triethylamine to form a 0.16 M solution followed by
57
58
59
60

1
2
3
4 the addition of alkyne (1.5-2 equiv.). The microwave vial was capped, and the reaction
5
6 mixture was stirred at 90 °C for 20 h. The cap was removed, and the reaction mixture was
7
8 diluted with ethyl acetate and filtered. The filtrate was washed with water, ammonium
9
10 chloride, and brine, dried with Na₂SO₄, and concentrated under reduced pressure. The crude
11
12 product mixture was purified by flash column chromatography to give **13i** and **13k**.

13
14 ***tert*-Butyl-3-(5-(2-(6-(2,5-dimethyl-1*H*-pyrrol-1-yl)-4-methylpyridin-2-yl)ethyl)pyridi-**
15
16 ***n*-3-yl)prop-2-ynyl(methyl)carbamate (**13i**)**. Compound **13i** was synthesized according to
17
18 general procedure **C** using Pd(PPh₃)₄ (28.8 mg), CuI (4.9 mg), alkyne **12i** (126.8 mg, 0.75
19
20 mmol), and **10** (184.6 mg, 0.50 mmol). **13i** was isolated as a brown oil (171.9 mg, 75%) after
21
22 flash column chromatography (MeOH: DCM 1:19). ¹H NMR (500 MHz, CDCl₃): δ 8.44 (s,
23
24 1H), 8.29 (s, 1H), 7.50 (s, 1H), 6.86 (s, 1H), 6.84 (s, 1H), 5.86 (s, 2H), 4.26 (brs, 2H),
25
26 3.05-3.04 (m, 4H), 2.94 (s, 3H), 2.33 (s, 3H), 2.08 (s, 6H), 1.46 (s, 9H); ¹³C NMR (125 MHz,
27
28 CDCl₃): δ 159.7, 151.8, 150.1, 149.7, 149.0, 148.6, 148.1, 138.6, 128.4, 122.7, 120.4, 119.6,
29
30 106.8, 88.0, 80.3, 80.2, 38.9, 38.8, 33.6, 32.3, 28.4, 21.0, 13.2; MS ESI: calcd. For
31
32 C₂₈H₃₅N₄O₂ [M+H]⁺, 459.28; found, 459.20.

33
34
35
36 **3-(5-(2-(6-(2,5-Dimethyl-1*H*-pyrrol-1-yl)-4-methylpyridin-2-yl)ethyl)pyridin-3-yl)-*N*,**
37
38 ***N*-dimethylprop-2-yn-1-amine (**13k**)**. Compound **13k** was synthesized according to general
39
40 procedure **C** using Pd(PPh₃)₄ (28.8 mg), CuI (5.1 mg), alkyne **12k** (62.3 mg), and **10** (185
41
42 mg). **13k** was isolated as a brown oil (166.6 mg, 90%) after flash column chromatography
43
44 (MeOH: DCM 1: 9). ¹H NMR (500 MHz, CDCl₃): δ 8.45 (s, 1H), 8.27 (s, 1H), 7.49 (s, 1H),
45
46 6.85 (s, 1H), 6.83 (s, 1H), 5.85 (s, 2H), 3.43 (s, 2H), 3.05-3.04 (m, 4H), 2.33 (s, 6H), 2.32 (s,
47
48 3H), 2.08 (s, 6H); ¹³C NMR (125 MHz, CDCl₃): δ 159.8, 151.8, 150.1, 149.7, 148.8, 138.6,
49
50 136.2, 128.4, 122.7, 120.4, 119.9, 106.7, 88.0, 82.1, 48.6, 44.3, 38.9, 32.3, 21.0, 13.2; MS
51
52 ESI: calcd. For C₂₄H₂₉N₄ [M+H]⁺, 373.24; found, 373.19.

53
54
55
56 **General Procedure D: Preparation of **11**, **14a-14e**, and **14g**, (Pyrrole Deprotection).** A
57
58 microwave vial was charged with **9**, **13a-13e**, or **13g** (1 equiv.) and NH₂OH·HCl (3-4 equiv.).
59
60

1
2
3
4 The mixtures were diluted with EtOH/water (2:1) to form a 0.16 M solution. The microwave
5 vial was capped, and the reaction mixture was stirred at 100 °C for 20 h. The cap was
6 removed, and the reaction mixture was concentrated under reduced pressure. The crude
7 product mixture was purified by flash chromatography to give **11**, **14a-14e**, and **14g**.

8
9
10
11 **6-(2-(5-(Dimethylamino)pyridin-3-yl)ethyl)-4-methylpyridin-2-amine (14a)**. **14a** was
12 synthesized according to general procedure **D** using **13a** (62.3 mg) and NH₂OH·HCl (52.7
13 mg). **14a** was isolated as a brown oil (47.2 mg, 99%) after flash column chromatography
14 (MeOH: DCM 4:6). ¹H NMR (500 MHz, methanol-*d*₄): δ 8.02 (s, 1H), 7.96 (s, 1H), 7.70 (s,
15 1H), 6.68 (s, 1H), 6.66 (s, 1H), 3.19-3.15 (m, 2H), 3.12-3.08 (m, 8H), 2.36 (s, 3H); ¹³C NMR
16 (125 MHz, Methanol-*d*₄): δ 157.6, 154.6, 148.1, 147.5, 139.6, 127.6, 125.4, 123.6, 113.7,
17 109.8, 38.7, 32.2, 31.4, 20.5; HRMS ESI: calcd. For C₁₅H₂₁N₄ [M+H]⁺, 257.1761; found,
18 251.1766.

19
20
21
22 **4-Methyl-6-(2-(5-(piperidin-1-yl)pyridin-3-yl)ethyl)pyridin-2-amine (14b)**. **14b** was
23 synthesized according to general procedure **D** using **13b** (62.8 mg) and NH₂OH·HCl (28.0
24 mg). **14b** was isolated as a brown oil (32.3 mg, 65%) after flash column chromatography
25 (MeOH: DCM 1:9). ¹H NMR (500 MHz, methanol-*d*₄): δ 8.18 (s, 1H), 7.96 (s, 1H), 7.76 (s,
26 1H), 6.70 (s, 1H), 6.66 (s, 1H), 3.37 (t, *J* = 5.0 Hz, 4H), 3.16-3.12 (m, 2H), 3.10-3.06 (m, 2H),
27 2.35 (s, 3H), 1.71-1.68 (m, 6H); ¹³C NMR (125 MHz, methanol-*d*₄): δ 157.5, 154.5, 148.5,
28 147.7, 138.7, 131.6, 128.8, 126.7, 113.7, 109.7, 48.2, 33.4, 31.4, 24.8, 23.6, 20.5; HRMS ESI:
29 calcd. For C₁₈H₂₅N₄ [M+H]⁺, 297.2074; found, 297.2078.

30
31
32
33 **4-Methyl-6-(2-(5-morpholinopyridin-3-yl)ethyl)pyridin-2-amine (14c)**. **14c** was
34 synthesized according to general procedure **D** using **13c** (82.8 mg, 0.50 mmol) and
35 NH₂OH·HCl (62.1 mg). **14c** was isolated as a brown oil (64.3 mg, 98%) after flash column
36 chromatography (MeOH: DCM 3:7). ¹H NMR (500 MHz, methanol-*d*₄): δ 8.31 (s, 1H), 8.17
37 (s, 1H), 8.14 (s, 1H), 6.72 (s, 1H), 6.71 (s, 1H), 3.86 (t, *J* = 5.0 Hz, 4H), 3.43 (t, *J* = 5.0 Hz,
38 4H), 3.25-3.22 (m, 2H), 3.15-3.12 (m, 2H), 2.37 (s, 3H); ¹³C NMR (125 MHz, methanol-*d*₄):
39
40
41
42
43
44
45
46
47
48
49
50
51
52
53
54
55
56
57
58
59
60

1
2
3
4
5
6
7
8
9
10
11
12
13
14
15
16
17
18
19
20
21
22
23
24
25
26
27
28
29
30
31
32
33
34
35
36
37
38
39
40
41
42
43
44
45
46
47
48
49
50
51
52
53
54
55
56
57
58
59
60

δ 157.7, 154.5, 149.1, 147.2, 140.5, 129.3, 129.2, 125.2, 113.8, 109.9, 65.8, 46.6, 33.0, 31.4, 20.6; HRMS ESI: calcd. For $C_{17}H_{23}N_4O$ $[M+H]^+$, 299.1866; found, 299.1872.

6-(2-(5-((2-Methoxyethyl)(methyl)amino)pyridin-3-yl)ethyl)-4-methylpyridin-2-amine (14d). **14d** was synthesized according to general procedure **D** using **13d** (61.8 mg) and $NH_2OH \cdot HCl$ (45.9 mg). **14d** was isolated as a brown oil (48.3 mg, 98%) after flash column chromatography (MeOH: DCM 3:7). 1H NMR (500 MHz, methanol- d_4): δ 8.11 (s, 1H), 8.01 (s, 1H), 7.87 (s, 1H), 6.73 (s, 1H), 6.71 (s, 1H), 3.72 (t, $J = 5.0$ Hz, 2H), 3.63 (t, $J = 5.0$ Hz, 2H), 3.32 (s, 3H), 3.23-3.20 (m, 2H), 3.15-3.12 (m, 5H), 2.36 (s, 3H); ^{13}C NMR (125 MHz, methanol- d_4): δ 157.7, 154.5, 147.9, 147.3, 140.0, 126.6, 126.5, 122.9, 113.8, 109.9, 70.0, 58.0, 51.4, 37.6, 33.1, 31.3, 20.6; HRMS ESI: calcd. For $C_{17}H_{25}N_4O$ $[M+H]^+$, 301.2023; found, 301.2031.

6-(2-(5-(3-Methoxypropylamino)pyridin-3-yl)ethyl)-4-methylpyridin-2-amine (14e). **14e** was synthesized according to general procedure **D** using **13e** (66.5 mg) and $NH_2OH \cdot HCl$ (50.2 mg). **14e** was isolated as a brown oil (49.1 mg, 93%) after flash column chromatography (MeOH: DCM 3:7). 1H NMR (500 MHz, methanol- d_4): δ 7.95 (s, 1H), 7.93 (s, 1H), 7.65 (s, 1H), 6.71 (s, 1H), 6.68 (s, 1H), 3.51 (t, $J = 6.0$ Hz, 2H), 3.35 (s, 3H), 3.29 (t, $J = 7.0$ Hz, 2H), 3.18-3.15 (m, 2H), 3.12-3.09 (m, 2H), 2.36 (s, 3H), 1.92-1.87 (m, 2H); ^{13}C NMR (125 MHz, methanol- d_4): δ 157.7, 154.5, 148.0, 147.2, 140.4, 127.0, 126.4, 122.4, 113.8, 109.9, 69.6, 57.6, 39.6, 32.9, 31.2, 28.3, 20.6; HRMS ESI: calcd. For $C_{17}H_{25}N_4O$ $[M+H]^+$, 301.2023; found, 301.2026.

4-Methyl-6-(2-(5-(4-methylpiperazin-1-yl)pyridin-3-yl)ethyl)pyridin-2-amine (14g). **14g** was synthesized according to general procedure **D** using **13g** (34.6 mg) and $NH_2OH \cdot HCl$ (25.1 mg). **14g** was isolated as a brown oil (18.0 mg, 65%) after flash column chromatography (MeOH: DCM 4:6). 1H NMR (500 MHz, methanol- d_4): δ 8.16 (s, 1H), 7.92 (s, 1H), 7.42 (s, 1H), 6.59 (s, 1H), 6.55 (s, 1H), 3.51-3.49 (m, 4H), 3.28-3.26 (m, 4H), 3.05-2.98 (m, 4H), 2.84 (s, 3H), 2.31 (s, 3H); ^{13}C NMR (125 MHz, methanol- d_4): δ 156.2,

1
2
3 155.3, 149.8, 146.3, 140.1, 136.6, 135.7, 123.9, 113.6, 109.1, 53.3, 46.1, 42.8, 34.5, 31.6,
4
5 20.4; HRMS ESI: calcd. For C₁₈H₂₆N₅ [M+H]⁺, 312.2183; found, 312.2186.
6
7

8 **General Procedure E: Preparation of 14j and 14k (Alkyne Reduction and Pyrrole**
9 **Deprotection).** A scintillation vial was charged with 10% wt. Pd/C and **13k** (1 equiv.). The
10 mixtures were diluted with methanol to form a 0.1 M solution. The reaction mixture was
11 stirred at r.t. for 20 h under hydrogen gas. At this time, the crude was filtered, and the filtrate
12 was concentrated under reduced pressure. The crude product was subjected to
13 2,5-dimethylpyrrole deprotection as described above (general procedure **D**) without
14 purification. A microwave vial was charged with the hydrogenation crude product (1 equiv.)
15 and NH₂OH·HCl (3-4 equiv.). The mixtures were diluted with EtOH/water (2:1) to form a
16 0.16 M solution. The microwave vial was capped, and the reaction mixture was stirred at 100
17 °C for 20 h. The cap was removed, and the reaction mixture was concentrated under reduced
18 pressure. The crude product mixture was purified by flash chromatography to give **14k**.
19
20
21
22
23
24
25
26
27
28
29
30
31

32 **6-(2-(5-(3-(Dimethylamino)propyl)pyridin-3-yl)ethyl)-4-methylpyridin-2-amine (14k).**
33 **14k** was synthesized according to general procedure **E** using **13k** (166.6 mg), 10% wt. Pd/C
34 (131.2 mg), and NH₂OH·HCl (79.2 mg). **14k** was isolated as a brown oil (118.5 mg, 89%)
35 after flash column chromatography (MeOH: DCM 4:6). ¹H NMR (500 MHz, methanol-*d*₄): δ
36 8.80 (s, 2H), 8.71 (s, 1H), 6.76 (s, 2H), 3.36-3.33 (m, 2H), 3.31-3.28 (m, 2H), 3.22-3.19 (m,
37 2H), 3.03-3.00 (m, 2H), 2.95 (s, 6H), 2.38 (s, 3H), 2.27-2.21 (m, 2H); ¹³C NMR (125 MHz,
38 methanol-*d*₄): δ 157.8, 154.5, 147.1, 147.0, 141.1, 140.4, 139.4, 139.1, 113.9, 110.0, 56.5,
39 42.2, 32.7, 31.1, 28.7, 24.8, 20.7; HRMS ESI: calcd. For C₁₈H₂₇N₄ [M+H]⁺, 299.2230; found,
40 299.2236.
41
42
43
44
45
46
47
48
49
50

51 **4-Methyl-6-(2-(5-(3-(methylamino)propyl)pyridin-3-yl)ethyl)pyridin-2-amine (14j).**
52 **14j** was synthesized by Boc deprotection of **13i** followed by general procedure **E**. Compound
53 **13i** (171.9 mg, 0.38 mmol) was diluted with DCM (3.8 ml) to form a 0.1 M solution followed
54 by addition of TFA (0.8 mL). The reaction mixture was allowed to stir at r.t. for 1 h. The
55
56
57
58
59
60

1
2
3
4
5
6
7
8
9
10
11
12
13
14
15
16
17
18
19
20
21
22
23
24
25
26
27
28
29
30
31
32
33
34
35
36
37
38
39
40
41
42
43
44
45
46
47
48
49
50
51
52
53
54
55
56
57
58
59
60

crude product was concentrated under reduced pressure, diluted with DCM, and washed with sat. NaHCO₃. The organic layer was dried over Na₂SO₄ and concentrated to give crude product **13j**. The crude product was used for further steps without purification. **14j** was synthesized according to general procedure **E** using **13j** (82.6 mg), 10% wt. Pd/C (56.1 mg), and NH₂OH·HCl (52.2 mg). **14j** was isolated as a brown oil (63.8 mg, 60%) after flash column chromatography (MeOH: DCM 4:6). ¹H NMR (500 MHz, methanol-*d*₄): δ 8.79 (s, 1H), 8.78 (s, 1H), 8.68 (s, 1H), 6.75 (s, 2H), 3.35-3.32 (m, 2H), 3.21-3.18 (m, 2H), 3.14-3.11 (m, 2H), 3.04-3.01 (m, 2H), 2.75 (s, 6H), 2.38 (s, 3H), 2.20-2.14 (m, 2H); ¹³C NMR (125 MHz, methanol-*d*₄): δ 157.8, 154.5, 147.1, 147.0, 141.2, 140.4, 139.4, 139.2, 113.9, 110.0, 48.1, 32.7, 32.4, 31.1, 28.8, 26.3, 20.7; HRMS ESI: calcd. For C₁₇H₂₅N₄ [M+H]⁺, 285.2074; found, 285.2078.

4-Methyl-6-(2-(5-(1-methylpiperidin-4-yl)pyridin-3-yl)ethyl)pyridin-2-amine (**14h**).

14h was synthesized by alkyne reduction of **13h** followed by Boc reduction and pyrrole deprotection. **13h** (316.2 mg) was treated with 10% wt. Pd/C (235.2 mg) and diluted with MeOH to form a 0.1 M solution. The reaction mixture was stirred at r.t. for 20 h under hydrogen gas. The crude product was filtered through Celite, and the filtrate was concentrated under reduced pressure. The crude product (298.9 mg) was subjected to *tert*-butyl carbamate reduction without purification. A round-bottom flask was charged with lithium aluminum hydride (126.1 mg), and the hydrogenation crude product solution in THF (0.1 M) was slowly added at 0 °C under N₂. The reaction mixture was allowed to warm up to r.t., refluxed for 1 h, quenched, with water, filtered, and extracted with dichloromethane to give the crude *tert*-butyl carbamate reduction product (136.6 mg), which was treated with NH₂OH·HCl (99.7 mg) and diluted with EtOH/water (2:1) to form a 0.16 M solution. The reaction mixture was stirred at 100 °C for 20 h, concentrated under reduced pressure, and purified by flash column chromatography to give **14h** (74.4 mg, 36%) as a brown oil. ¹H NMR (500 MHz, methanol-*d*₄): δ 8.35 (s, 1H), 8.32 (s, 1H), 7.74 (s, 1H), 6.60 (s, 1H), 6.54 (s, 1H), 3.62-3.60

1
2
3 (m, 2H), 3.22-3.20 (m, 3H), 3.08-3.07 (m, 2H), 3.04-2.98 (m, 4H), 2.93 (s, 3H), 2.88-2.86 (m,
4
5 2H), 2.29 (s, 3H); ^{13}C NMR (125 MHz, methanol- d_4): δ 155.8, 155.6, 150.1, 147.4, 145.8,
6
7 139.7, 136.5, 135.4, 113.7, 109.0, 54.1, 48.5, 42.5, 34.7, 31.6, 29.9, 20.4; HRMS ESI: calcd.
8
9 For $\text{C}_{19}\text{H}_{27}\text{N}_4$ $[\text{M}+\text{H}]^+$, 311.2230; found, 311.2231.

10
11
12 **NOS Enzyme Inhibition Assays.** Enzyme inhibition was evaluated by measuring NO
13
14 production with the hemoglobin capture assay, which was performed with purified NOSs in
15
16 96-well plates using a Biotek Gen5TM microplate reader. Purified NOSs used in this study, rat
17
18 nNOS, human nNOS, murine macrophage iNOS, bovine eNOS, and human eNOS, are
19
20 recombinant enzymes, expressed in *E. coli* and purified by reported procedures.³⁷⁻³⁹ For rat
21
22 and human nNOS, bovine and human eNOS, the assays were performed at 37 °C in 100 mM
23
24 HEPES buffer with 10% glycerol (pH 7.4) in the presence of 10 μM *L*-arginine and
25
26 tetrahydrobiopterin, 100 μM NADPH, 0.83 mM CaCl_2 , 320 units/mL of calmodulin, and 3
27
28 μM human oxyhemoglobin. For iNOS, the assay was performed at 37 °C in HEPES buffer in
29
30 the presence of *L*-arginine and cofactors (NADPH, H_4B , and human oxyhemoglobin). For all
31
32 the assays, NO production was read by monitoring the absorbance at 401 nm, and kinetic
33
34 readouts were recorded for 6 min. The inhibition constants (K_i) for all NOSs were calculated
35
36 from the IC_{50} values and K_m (human nNOS: 1.6 μM ; rat nNOS: 1.3 μM ; murine iNOS: 8.2
37
38 μM ; bovine eNOS: 1.7 μM ; human eNOS: 3.9 μM)⁴⁰ using the Cheng–Prusoff equation:
39
40 $K_i = \text{IC}_{50} / (1 + [\text{S}] / K_m)$.⁴¹ IC_{50} values were determined with seven to nine concentration points
41
42 (200 μM –50 nM) to construct dose–response curves, and were calculated by nonlinear
43
44 regression using GraphPad Prism. The calculated standard deviations of the assays were less
45
46 than 10% with all NOSs using dose-response curves.

47
48
49 **Inhibitor Complex Crystal Preparation.** The preparations of rat nNOS, bovine eNOS,
50
51 human eNOS, and human nNOS heme domains used for crystallographic studies were carried
52
53 out using procedures described previously.^{24,42,43} The rat nNOS heme domain (at 9 mg/mL
54
55 containing 20 mM histidine) or the bovine eNOS heme domain (at 10 mg/mL containing 2
56
57
58
59
60

1
2
3
4 mM imidazole) were used for the sitting drop vapor diffusion crystallization setup under
5
6 conditions previously reported.⁴² Human nNOS crystals were obtained with a triple
7
8 K301R/R354A/G357D mutant heme domain at 10 mg/mL. By slightly modifying the original
9
10 conditions where the monoclinic C2 crystals grew, a new crystal form belonging to the
11
12 P2₁2₁2₁ space group was obtained. Long plate crystals were grown at 4 °C with the sitting
13
14 drop setup against a well solution of 8-9% PEG3350, 40 mM citric acid, 60 mM
15
16 Bis-Tris-Propane, pH 6.2, 10% glycerol, and 5 mM TCEP. New crystals belong to the
17
18 orthorhombic P2₁2₁2₁ space group with cell dimensions of a= 52.3 Å, b= 122.7 Å, and c=
19
20 165.0 Å with one homodimer in the asymmetric unit, which closely resembles the cell
21
22 dimensions of rat nNOS crystal. Fresh crystals were first passed stepwise through
23
24 cryoprotectant solutions and then soaked with 10 mM inhibitor for 4–6 h at 4 °C before being
25
26 flash cooled in liquid nitrogen.
27
28

29
30 **X-ray Diffraction Data Collection, Data Processing, and Structural Refinement.** The
31
32 cryogenic (100 K) X-ray diffraction data were collected remotely at the Stanford Synchrotron
33
34 Radiation Light source (SSRL) or Advanced Light Source (ALS) through the data collection
35
36 control software Blu-Ice⁴⁴ and a crystal mounting robot. When a Q315r CCD detector was
37
38 used, 90–100° of data were typically collected with 0.5° per frame. If a Pilatus pixel array
39
40 detector was used, 120–130° of fine-sliced data were collected with 0.2° per frame. Raw
41
42 CCD data frames were indexed, integrated, and scaled using MOSFLM,⁴⁵ but the pixel array
43
44 data were processed with XDS⁴⁶ and scaled with or Aimless.⁴⁷ The binding of inhibitors was
45
46 detected by the initial difference Fourier maps calculated with REFMAC.⁴⁸ The inhibitor
47
48 molecules were then modeled in COOT⁴⁹ and refined using REFMAC or PHENIX.⁵⁰
49
50 Disordering in portions of inhibitors bound in the NOS active sites was often observed,
51
52 sometimes resulting in poor density quality. However, partial structural features usually could
53
54 still be visible if the contour level of the sigma A weighted $2m|F_o|-D|F_c|$ map dropped to 0.5
55
56 σ , which afforded the building of reasonable models into the disordered regions. Water
57
58
59
60

1
2
3 molecules were added in PHENIX and checked by COOT. The TLS⁵¹ protocol was
4 implemented in the final stage of refinements with each subunit as one TLS group. The omit
5 $F_o - F_c$ density maps shown in figures were calculated by running one round of simulated
6 annealing refinement (initial temperature 2000 K) in PHENIX with the inhibitor coordinate
7 removed from the input PDB file to generate map coefficients DELFWT and PHDELWT.
8 The refined structures were validated in COOT before deposition in the RCSB protein data
9 bank. The crystallographic data collection and structure refinement statistics are summarized
10 in Table S1 of the Supporting Information, with the PDB accession codes included.
11
12
13
14
15
16
17
18
19
20
21
22

23 ASSOCIATED CONTENT

24 Supporting Information

25 Preparation of compounds **7**, **8a**, **8b**, **12h**, and **12i**

26 Crystallographic data collection and structure refinement statistics.

27 CYP inhibition protocol.

28 Biological assays for **14j** (Metabolic stability in HLM, Determination of protein binding in
29 human plasma, and Caco-2 permeability)

30 This material is available free of charge via the Internet at <http://pubs.acs.org>.

31 Accession Codes

32 PDB codes for structures reported here: nNOS-**14c**, 5FVP; nNOS-**14d**, 5FW0; nNOS-**14e**,
33 5FVO; nNOS-**14g**, 5FVQ; nNOS-**14h**, 5FVR; nNOS-**14j**, 5FVS; nNOS-**14k**, 5FVT;
34 HnNOS-**14g**, 5FVU; HnNOS-**14h**, 5FVV; HnNOS-**14j**, 5FVW; HnNOS-**14k**, 5FVX;
35 eNOS-**14g**, 5FVY; eNOS-**14k**, 5FVZ. Authors will release the atomic coordinates and
36 experimental data upon article publication.
37
38
39
40
41
42
43
44
45
46
47
48
49
50
51
52
53
54
55
56
57

58 AUTHOR INFORMATION

Corresponding Authors

*(T.L.P.) Tel:+1 949 824 7020. E-mail: poulos@uci.edu.

*(R.B.S.) Tel:+1 847 491 5653. Fax: +1 847 491 7713.

E-mail:Agman@chem.northwestern.edu.

Notes

The authors declare no competing financial interest.

ACKNOWLEDGMENTS

The authors are grateful for financial support from the National Institutes of Health (GM049725 to R.B.S. and GM057353 to T.L.P.). Y.J.Q. is funded by the China Scholarship Council. L.J.R. is currently supported on NIH GM081568 and NSF grant 13-573. P.M. is supported by grants UNCE 204011 and PRVOUK P24/LF1/3 from Charles University, Prague, Czech Republic. H-Y.W. and Y.J.Q. wish to thank Mr. Saman Shafaie and Dr. S. Habibi Goudarzi in Northwestern's Integrated Molecular Structure Education and Research Center for assistance with HRMS experiments. We also wish to thank the SSRL and ALS beamline staff for their support during X-ray diffraction and data collection.

ABBREVIATIONS USED

NO, nitric oxide; nNOS, neuronal nitric oxide synthase; iNOS, inducible nitric oxide synthase; eNOS, endothelial nitric oxide synthase; HnNOS, human neuronal nitric oxide synthase; HeNOS, human endothelial nitric oxide synthase; *L*-Arg, *L*-arginine; FAD, flavin adenine dinucleotide; FMN, flavin mononucleotide; NADPH, reduced nicotinamide adenine dinucleotide phosphate; H₄B, (6*R*)-5,6,7,8-tetrahydrobiopterin; HEPES, 4-(2-hydroxyethyl)-1-piperazine-ethanesulfonic acid; TCEP, tris(2-chloroethyl)phosphate; WT, wild type.

REFERENCES

- (1) Kerwin, J. F., Jr.; Lancaster, J. R., Jr.; Feldman, P. L. Nitric oxide: a new paradigm for second messengers. *J. Med. Chem.* **1995**, *38*, 4343-4362.
- (2) Palmer, R. M.; Ferrige, A. G.; Moncada, S. Nitric oxide release accounts for the biological activity of endothelium-derived relaxing factor. *Nature* **1987**, *327*, 524-526.
- (3) Ignarro, L. J.; Lippton, H.; Edwards, J. C.; Baricos, W. H.; Hyman, A. L.; Kadowitz, P. J.; Gruetter, C. A. Mechanism of vascular smooth muscle relaxation by organic nitrates, nitrites, nitroprusside and nitric oxide: evidence for the involvement of S-nitrosothiols as active intermediates. *J. Pharmacol. Exp. Ther.* **1981**, *218*, 739-749.
- (4) Vincent, S. R. Nitric oxide: a radical neurotransmitter in the central nervous system. *Prog. Neurobiol.* **1994**, *42*, 129-160.
- (5) Bogdan, C. Nitric oxide and the immune response. *Nat. Immunol.* **2001**, *2*, 907-916.
- (6) Karpuzoglu, E.; Ahmed, S. A. Estrogen regulation of nitric oxide and inducible nitric oxide synthase (iNOS) in immune cells: implications for immunity, autoimmune diseases, and apoptosis. *Nitric Oxide* **2006**, *15*, 177-186.
- (7) Roe, N. D.; Ren, J. Nitric oxide synthase uncoupling: a therapeutic target in cardiovascular diseases. *Vasc. Pharmacol.* **2012**, *57*, 168-172.
- (8) Baranano, D. E.; Snyder, S. H. Neural roles for heme oxygenase: contrasts to nitric oxide synthase. *Proc. Natl. Acad. Sci. U.S.A.* **2001**, *98*, 10996-1002.
- (9) Steinert, J. R.; Chernova, T.; Forsythe, I. D. Nitric oxide signaling in brain function, dysfunction, and dementia. *Neuroscientist* **2010**, *16*, 435-452.
- (10) Huang, H.; Ji, H.; Li, H.; Jing, Q.; Labby, K. J.; Martasek, P.; Roman, L. J.; Poulos, T. L.; Silverman, R. B. Selective monocationic inhibitors of neuronal nitric oxide synthase. Binding mode insights from molecular dynamics simulations. *J. Am. Chem. Soc.* **2012**, *134*, 11559-11572.

- 1
2
3 (11) Law, A.; Gauthier, S.; Quirion, R. Say NO to Alzheimer's disease: the putative links
4 between nitric oxide and dementia of the Alzheimer's type. *Brain Res. Brain Res. Rev.* **2001**,
5 *35*, 73-96.
6
7
8
9
10 (12) Aquilano, K.; Baldelli, S.; Rotilio, G.; Ciriolo, M. R., Role of nitric oxide synthases in
11 Parkinson's disease: a review on the antioxidant and anti-inflammatory activity of
12 polyphenols. *Neurochem. Res.* **2008**, *33*, 2416-26.
13
14
15
16 (13) Deckel, A. W.; Tang, V.; Nuttal, D.; Gary, K.; Elder, R. Altered neuronal nitric oxide
17 synthase expression contributes to disease progression in Huntington's disease transgenic
18 mice. *Brain Res.* **2002**, *939*, 76-86.
19
20
21
22 (14) Yamanaka, K.; Chun, S. J.; Boillee, S.; Fujimori-Tonou, N.; Yamashita, H.; Gutmann, D.
23 H.; Takahashi, R.; Misawa, H.; Cleveland, D. W. Astrocytes as determinants of disease
24 progression in inherited amyotrophic lateral sclerosis. *Nat. Neurosci.* **2008**, *11*, 251-253.
25
26
27
28 (15) Baek, K. J.; Thiel, B. A.; Lucas, S.; Stuehr, D. J. Macrophage nitric oxide synthase
29 subunits. purification, characterization, and role of prosthetic groups and substrate in
30 regulating their association into a dimeric enzyme. *J. Biol. Chem.* **1993**, *268*, 21120-21129.
31
32
33
34 (16) Mukherjee, P.; Cinelli, M. A.; Kang, S.; Silverman, R. B. Development of nitric oxide
35 synthase inhibitors for neurodegeneration and neuropathic pain. *Chem. Soc. Rev.* **2014**, *43*,
36 6814-6838.
37
38
39
40 (17) Alderton, W. K.; Cooper, C. E.; Knowles, R. G. Nitric oxide synthases: structure,
41 function and inhibition. *Biochem. J.* **2001**, *357*, 593-615.
42
43
44 (18) Feng, C. Mechanism of Nitric Oxide Synthase regulation: electron transfer and
45 interdomain interactions. *Coord. Chem. Rev.* **2012**, *256*, 393-411.
46
47
48
49 (19) Poulos, T. L.; Li, H. Structural basis for isoform-selective inhibition in nitric oxide
50 synthase. *Acc. Chem. Res.* **2013**, *46*, 390-398.
51
52
53
54 (20) Annedi, S. C.; Ramnauth, J.; Maddaford, S. P.; Renton, P.; Rakhit, S.; Mladenova, G.;

1
2
3 Dove, P.; Silverman, S.; Andrews, J. S.; Felice, M. D.; Porreca, F. Discovery of
4 *cis-N*-(1-(4-(methylamino)cyclohexyl)indolin-6-yl)thiophene-2-carboximidamide: A
5
6
7 1,6-disubstituted indoline derivative as a highly selective inhibitor of human neuronal nitric
8
9
10
11
12
13
14
15
16
17
18
19
20
21
22
23
24
25
26
27
28
29
30
31
32
33
34
35
36
37
38
39
40
41
42
43
44
45
46
47
48
49
50
51
52
53
54
55
56
57
58
59
60

oxide synthase (nNOS) without any cardiovascular liabilities. *J. Med. Chem.* **2012**, *55*, 943-955.

(21) Suaifan, G. A.; Shehadeh, M.; Al-Ijel, H.; Taha, M. O. Extensive ligand-based modeling and in silico screening reveal nanomolar inducible nitric oxide synthase (iNOS) inhibitors. *J. Mol. Graphics* **2012**, *37*, 1-26.

(22) Ji, H.; Tan, S.; Igarashi, J.; Li, H.; Derrick, M.; Martasek, P.; Roman, L. J.; Vasquez-Vivar, J.; Poulos, T. L.; Silverman, R. B. Selective neuronal nitric oxide synthase inhibitors and the prevention of cerebral palsy. *Ann. Neurol.* **2009**, *65*, 209-217.

(23) Xue, F.; Fang, J.; Delker, S. L.; Li, H.; Martasek, P.; Roman, L. J.; Poulos, T. L.; Silverman, R. B. Symmetric double-headed aminopyridines, a novel strategy for potent and membrane-permeable inhibitors of neuronal nitric oxide synthase. *J. Med. Chem.* **2011**, *54*, 2039-2048.

(24) Kang, S.; Li, H.; Tang, W.; Martasek, P.; Roman, L. J.; Poulos, T. L.; Silverman, R. B. 2-Aminopyridines with a truncated side chain to improve human neuronal Nitric Oxide Synthase inhibitory potency and selectivity. *J. Med. Chem.* **2015**, *58*, 5548-5560.

(25) Examples for amidine inhibitors:

Zhang, H. Q.; Fast, W.; Marletta, M. A.; Martásek, P.; Silverman, R. B. Potent and selective inhibition of neuronal nitric oxide synthase by *N*^ω-propyl-L-arginine. *J. Med. Chem.* **1997**, *40*, 3869-3870.

(26) Examples for dipeptide inhibitors:

1
2
3 Ji, H.; Gómez-Vidal, J. A.; Martásek, P.; J. Roman, L. J.; Silverman, R. B.
4
5 Conformationally-restricted dipeptide amides as potent and selective neuronal nitric oxide
6
7 synthase inhibitors. *J. Med. Chem.* **2006**, *49*, 6254–6263.
8

9
10 (27) Examples for thiophene inhibitors:

11
12 Huang, H.; Li, H.; Yang, S.; Chreifi, G.; Martásek, P.; Roman, L. J.; Meyskens, F. L.; Poulos,
13
14 T. L.; Silverman, R. B. Potent and selective double-headed thiophene-2-carboximidamide
15
16 inhibitors of neuronal nitric oxide synthase for the treatment of melanoma. *J. Med. Chem.*
17
18 **2014**, *57*, 686–700.
19

20
21 (28) Examples for aminopyridine inhibitors:

22
23 Huang, H.; Li, H.; Martásek, P.; Roman, L. J.; Poulos, T. L.; Silverman, R. B.
24
25 Structure-guided design of selective inhibitors of neuronal nitric oxide synthase. *J. Med.*
26
27 *Chem.* **2013**, *56*, 3024–3032.
28

29
30 (29) Examples for aminoquinoline inhibitors:

31
32 (a) Cinelli, M. A.; Li, H.; Chreifi, G.; Martásek, P.; Roman, L. J.; Poulos, T. L.; Silverman,
33
34 R. B. A simplified 2-aminoquinoline-based scaffold for potent and selective neuronal nitric
35
36 oxide synthase inhibition. *J. Med. Chem.* **2014**, *57*, 1513–1530. (b) Cinelli, M. A.; Li, H.;
37
38 Pensa, A. V.; Kang, S.; Roman, L. J.; Martasek, P.; Poulos, T. L.; Silverman, R. B. Phenyl
39
40 ether- and aniline-containing 2-aminoquinolines as potent and selective inhibitors of neuronal
41
42 nitric oxide synthase. *J. Med. Chem.* **2015**, *58*, 8694–8712.
43
44

45
46 (30) Examples for 2,4-disubstituted pyrimidines inhibitors:

47
48 Mukherjee, P.; Li, H.; Sevrioukova, I.; Chreifi, G.; Martásek, P.; Roman, L. J.; Poulos, T. L.;
49
50 Silverman, R. B. Novel 2,4-disubstituted pyrimidines as potent, selective, and cell-permeable
51
52 inhibitors of neuronal Nitric Oxide Synthase. *J. Med. Chem.* **2015**, *58*, 1067–1088.
53

54
55 (31) Surry, D. S.; Buchwald, S. L. Dialkylbiaryl phosphines in Pd-catalyzed amination: A
56
57 user's guide. *Chem. Sci.* **2011**, *2*, 27–50.
58
59
60

- 1
2
3 (32) (a) Zhang, M.; Cui, X.; Chen, X.; Wang, L.; Li, J.; Wu, Y.; Hou, L.; Wu, Y. Facile
4 synthesis of aryl(het)cyclopropane catalyzed by palladacycle. *Tetrahedron* **2012**, *68*, 900–905.
5
6
7 (b) Wallace, D. J.; Chen, C.-Y. Cyclopropyl boronic acid: synthesis and Suzuki
8 cross-coupling reactions. *Tetrahedron Lett.* **2002**, *43*, 6987–6990.
9
10
11 (33) Nakamura, H.; Onagi, S.; Kamakura, T. Synthesis of heterocyclic allenes *via*
12 palladium-catalyzed hydride-transfer reaction of propargylic amines. *J. Org. Chem.* **2005**, *70*,
13 2357-2360.
14
15
16 (34) Labby, K. J.; Xue, F.; Kraus, J. M.; Ji, H.; Mataka, J.; Li, H.; Martásek, P.; Roman, L. J.;
17 Poulos, T. L.; Silverman, R. B. Intramolecular hydrogen bonding: A potential strategy for
18 more bioavailable inhibitors of neuronal nitric oxide synthase. *Bioorg. Med. Chem.* **2012**, *20*,
19 2435–2443.
20
21
22 (35) Hevel, J. M.; Marletta, M. A. Nitric-oxide synthase assays. *Methods Enzymol.* **1994**, *233*,
23 250–258.
24
25
26 (36) Li, H.; Jamal, J.; Plaza, C.; Pineda, S. H.; Chreifi, G.; Jing, Q.; Cinelli, M. A.; Silverman,
27 R. B.; Poulos, T. L. Crystal structures of human constitutive nitric oxide synthases. *Acta*
28 *Crystallogr. Sect. D: Biol. Crystallogr.* **2014**, *70*, 2667–2674.
29
30
31 (37) Roman, L. J.; Sheta, E. A.; Martásek, P.; Gross, S. S.; Liu, Q.; Masters, B. S. S.
32 High-level expression of functional rat neuronal nitric oxide synthase in *Escherichia coli*.
33 *Proc. Natl. Acad. Sci. U. S. A.* **1995**, *92*, 8428–8432.
34
35
36 (38) Hevel, J. M.; White, K. A.; Marletta, M. A. Purification of the inducible murine
37 macrophage nitric oxide synthase: identification as a flavin protein. *J. Biol. Chem.* **1991**, *266*,
38 22789–22791.
39
40
41 (39) Gerber, N. C.; Ortiz de Montellano, P. R. Neuronal nitric oxide synthase: expression in
42 *Escherichia coli*, irreversible inhibition by phenyldiazene, and active site topology. *J. Biol.*
43 *Chem.* **1995**, *270*, 17791–17796.
44
45
46
47
48
49
50
51
52
53
54
55
56
57
58
59
60

1
2
3 (40) Delker, S. L.; Xue, F.; Li, H.; Jamal, J.; Silverman, R. B.; Poulos, T. L. Role of zinc in
4 isoform-selective inhibitor binding to neuronal nitric oxide synthase. *Biochemistry* **2010**, *49*,
5 10803–10810.
6
7

8
9 (41) Cheng, Y.-C.; Prusoff, W. H. Relationship between the inhibition constant (K_i) and the
10 concentration of the inhibitor which causes 50% inhibition (IC_{50}) of an enzymatic reaction.
11 *Biochem. Pharmacol.* **1973**, *22*, 3099–3108.
12
13

14 (42) Li, H.; Jamal, J.; Delker, S.; Plaza, C.; Ji, H.; Jing, Q.; Huang, H.; Kang, S.; Silverman,
15 R. B.; Poulos, T. L. The mobility of a conserved tyrosine residue controls isoform-dependent
16 enzyme-inhibitor interaction in nitric oxide synthases. *Biochemistry* **2014**, *53*, 5272–5279.
17
18

19 (43) Labby, K. J.; Xue, F.; Kraus, J. M.; Ji, H.; Mataka, J.; Li, H.; Martásek, P.; Roman, L. J.;
20 Poulos, T. L.; Silverman, R. B. Intramolecular hydrogen bonding: A potential strategy for
21 more bioavailable inhibitors of neuronal nitric oxide synthase. *Bioorg. Med. Chem.* **2012**, *20*,
22 2435–2443.
23
24

25 (44) McPhillips, T. M.; McPhillips, S. E.; Chiu, H. J.; Cohen, A. E.; Deacon, A. M.; Ellis, P.
26 J.; Garman, E.; Gonzalez, A.; Sauter, N. K.; Phizackerley, R. P.; Soltis, S. M.; Kuhn, P.
27 Blu-Ice and the distributed control system: software for data acquisition and instrument
28 control at macromolecular crystallography beamlines. *J. Synchrotron Radiat.* **2002**, *9*,
29 401–406.
30
31

32 (45) Leslie, A. G. W.; Powell, H.R. Processing diffraction data with Mosflm. In *Evolving*
33 *Methods for Macromolecular Crystallography*; Read, R. J., Sussman, J. L., Eds.; Springer:
34 the Netherlands, 2007, Vol. 245, pp 41-51.
35
36

37 (46) Kabsch, W. XDS. *Acta Crystallogr. Sect. D: Biol. Crystallogr.* **2010**, *D66*, 125–132.
38
39

40 (47) Evans, P. R. Scaling and assessment of data quality. *Acta Crystallogr. Sect D: Biol.*
41 *Crystallogr.* **2006**, *D62*, 72–82.
42
43

44 (48) Murshudov, G. N.; Vagin, A. A.; Dodson, E. J. Refinement of macromolecular
45
46
47
48
49
50
51
52
53
54
55
56
57
58
59
60

1
2
3 structures by the maximum-likelihood method. *Acta Crystallogr. Sect. D: Biol. Crystallogr.*
4
5 **1997**, *D53*, 240–255.

6
7 (49) Emsley, P.; Cowtan, K. Coot: model-building tools for molecular graphics. *Acta*
8
9 *Crystallogr. Sect. D: Biol. Crystallogr.* **2004**, *D60*, 2126–2132.

10
11 (50) Adams, P. D.; Afonine, P. V.; Bunkóczi, G.; Chen, V. B.; Davis, I. W.; Echols, N.; Headd,
12
13 J. J.; Hung, L.-W.; Kapral, G. J.; Grosse-Kunstleve, R. W.; McCoy, A. J.; Moriarty, N. W.;
14
15 Oeffner, R.; Read, R. J.; Richardson, D. C.; Richardson, J. S.; Terwilliger, T. C.; Zwart, P. H.
16
17 PHENIX: a comprehensive Python-based system for macromolecular structure solution. *Acta*
18
19 *Crystallogr.* **2010**, *D66*, 213-221.

20
21 (51) Winn, M. D.; Isupov, M. N.; Murshudov, G. N. Use of TLS parameters to model
22
23 anisotropic displacements in macromolecular refinement. *Acta Crystallogr. Sect. D: Biol.*
24
25 *Crystallogr.* **2001**, *D57*, 122–133.
26
27
28
29
30
31
32
33
34
35
36
37
38
39
40
41
42
43
44
45
46
47
48
49
50
51
52
53
54
55
56
57
58
59
60

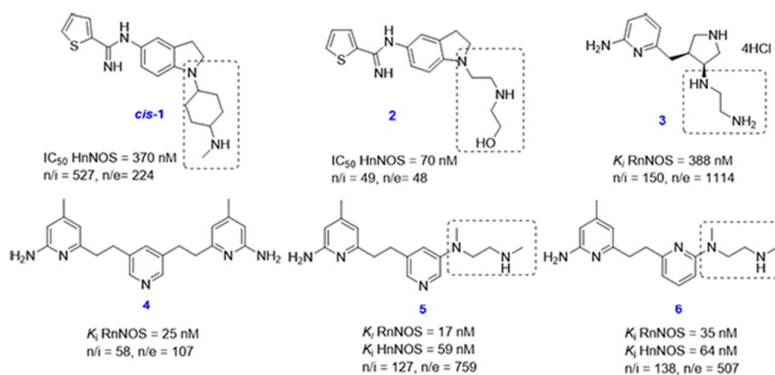


Figure 1. Representative nNOS inhibitors that share similar pharmacophores

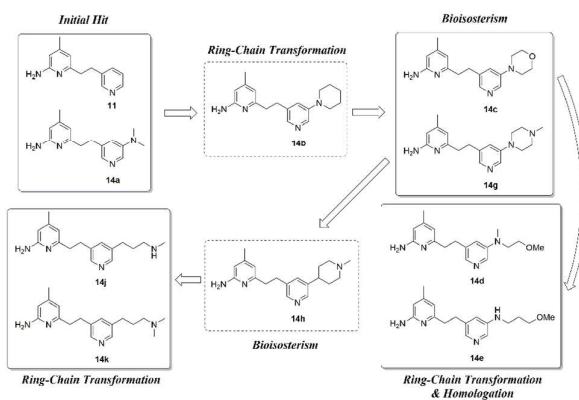


Figure 2. nNOS inhibitors design strategy in this study

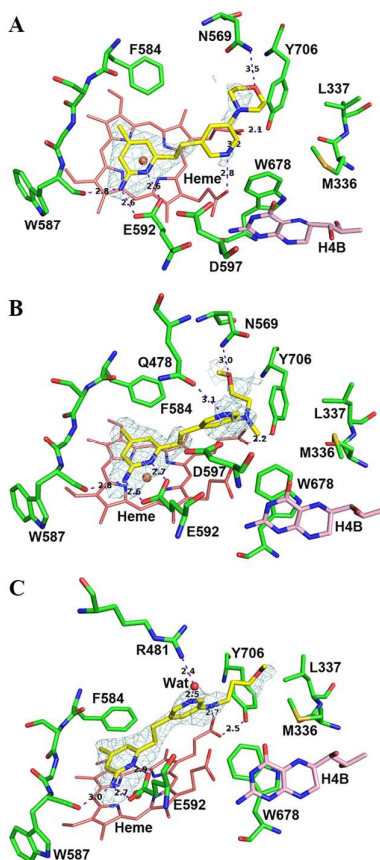


Figure 3. Active site structure of **14c** (A) (PDB 5FVP), **14d** (B) (PDB 5FW0) or **14e** (C) (PDB 5FVO) bound to nNOS. The omit $F_o - F_c$ electron density for the inhibitor is shown at the 2.5σ contour level. Major hydrogen bonds are depicted with dashed lines and distances are shown in Å.

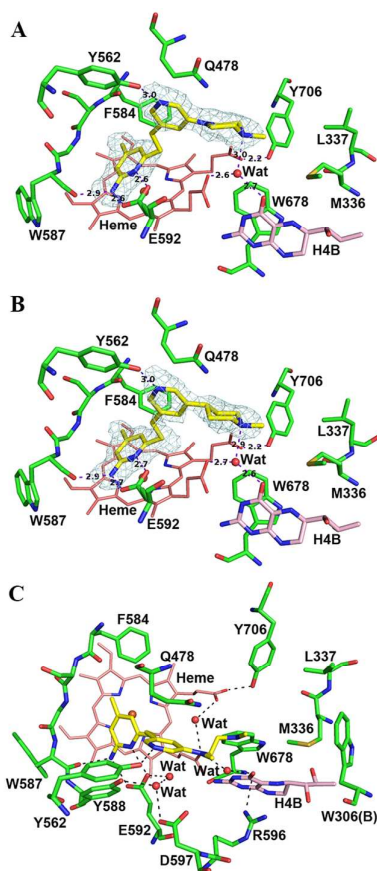


Figure 4. Active site structure of **14g** (A) (PDB 5FVQ) or **14h** (B) (PDB 5FVR) bound to nNOS. The omit $F_o - F_c$ electron density for the inhibitor is shown at the 2.5σ contour level. Major hydrogen bonds are depicted with dashed lines and distances are marked in Å. For comparison, panel C also shows the active site structure of **5** (PDB 4UH1) bound to nNOS.

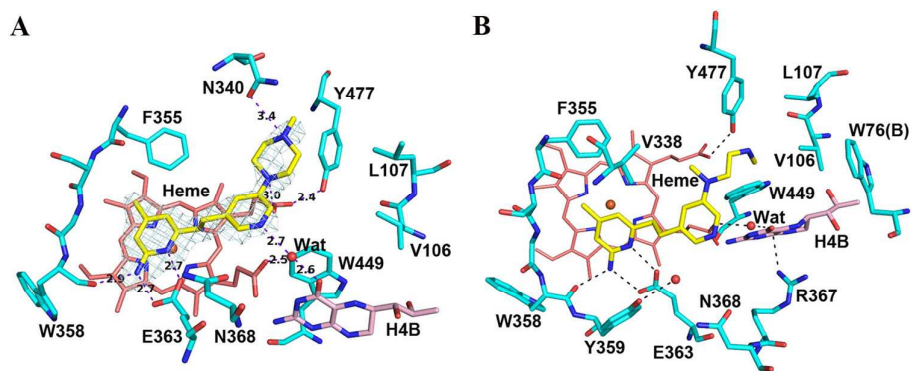


Figure 5. (A) Active site structure of **14g** (PDB 5FVY) bound to bovine eNOS. The omit $F_o - F_c$ electron density for the inhibitor is shown at the 2.5 σ contour level. (B) Active site structure of **5** (PDB 4UH8) bound to bovine eNOS. Major hydrogen bonds are depicted with dashed lines, and distances are marked in Å.

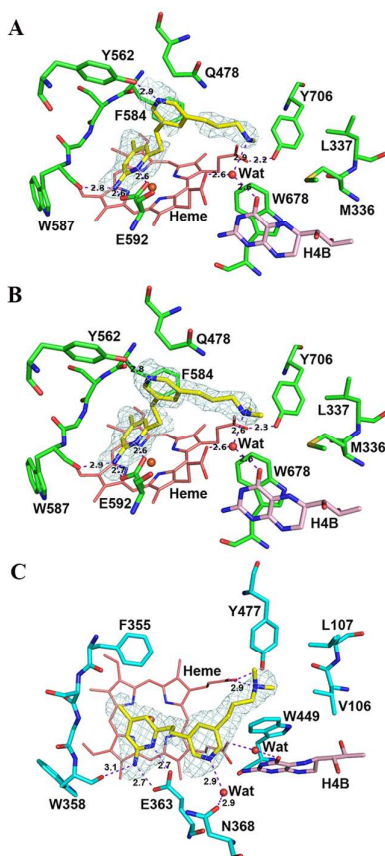


Figure 6. Active site structure of **14j** (A) (PDB 5FVS) or **14k** (B) (PDB 5FVT) bound to nNOS. Active site structure of **14k** (C) (PDB 5FVZ) bound to eNOS. The omit $F_o - F_c$ electron density for the inhibitor is shown at the 2.5σ contour level. Major hydrogen bonds are depicted with dashed lines, and distances are marked in Å.

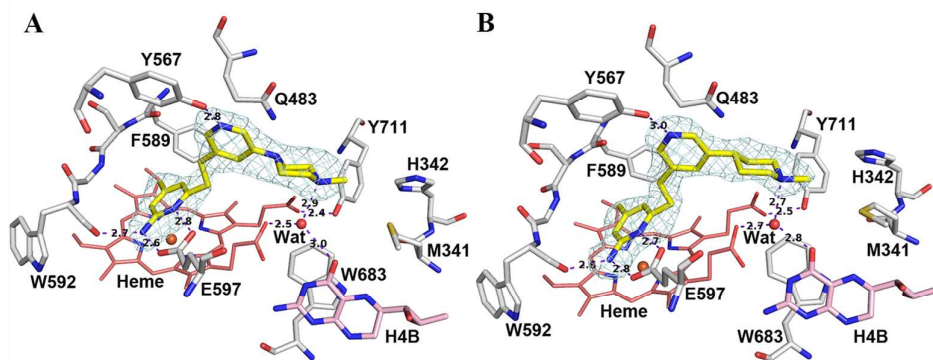


Figure 7. Active site structure of **14g** (A) (PDB 5FVU) or **14h** (B) (PDB 5FVV) bound to human nNOS. The omit $F_o - F_c$ electron density for the inhibitor is shown at the 2.5σ contour level. Major hydrogen bonds are depicted with dashed lines, and distances are marked in Å.

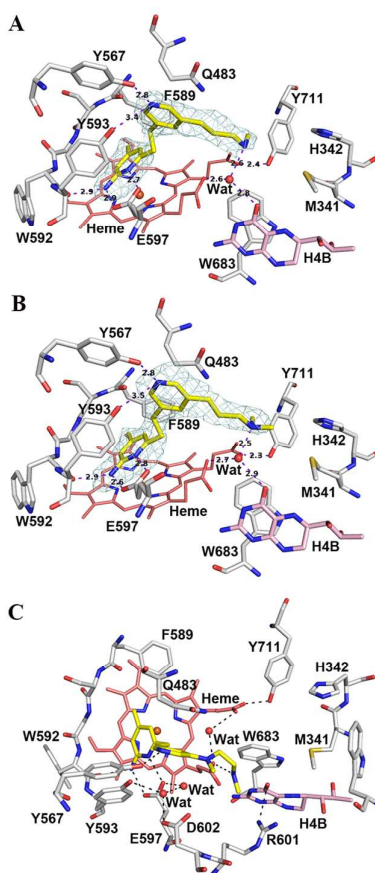
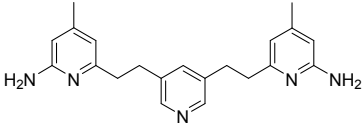
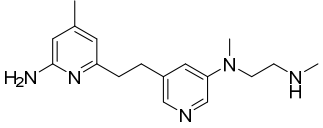
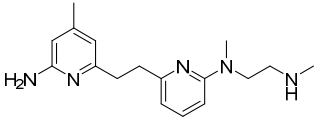
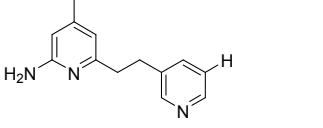
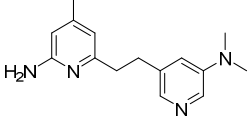
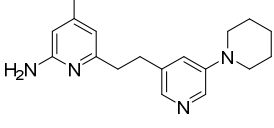
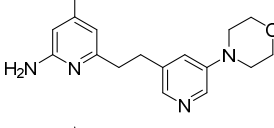
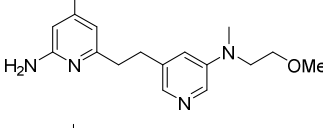
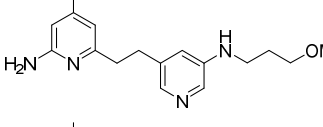
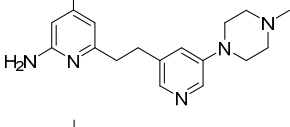
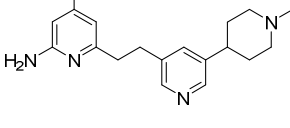
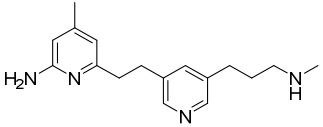
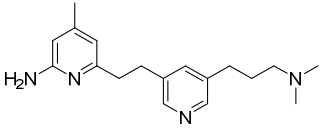


Figure 8. Active site structure of **14j** (A) (PDB 5FVW) or **14k** (B) (PDB 5FVX) bound to human nNOS. The omit $F_o - F_c$ electron density for the inhibitor is shown at the 2.5 σ contour level. Major hydrogen bonds are depicted with dashed lines, and distances are marked in Å. For comparison, panel (C) also shows active site structure of **5** (PDB 4UH5) bound to human nNOS.

Table 1. Inhibition of non-human NOSs by 4-6, 11, 14a-14e, 14g-14h, 14j, and 14k

Cmpd	Structure	K_i (nM) ^a			Selectivity ^b	
		nNOS	iNOS	eNOS	n/i	n/e
4		25	1450	2680	58	107
5		17	2152	12910	127	759
6		35	4845	17742	138	507
11		706	2784	NT ^c	4	NA ^d
14a		139	1797	NT	13	NA
14b		1875	5642	NT	3	NA
14c		547	11570	NT	21	NA
14d		1768	18233	NT	10	NA
14e		558	7053	NT	13	NA
14g		43	14214	> 30000	331	>698
14h		72	11779	20487	164	285

14j		16	1894	13247	118	828
14k		25	1486	16637	59	665

^a K_i values are calculated directly from IC_{50} values. IC_{50} values are the average of at least two replicates from nine data points. All experimental standard error values are less than 15%.

^bSelectivity values are determined by calculating the ratios of respective K_i values.

^cNT = not tested

^dNA = not applicable

Table 2. Inhibition of human nNOS by 5, 6, 14a, 14c, 14g, 14h, 14j, and 14k

Cmpd	K_i (nM) ^a		Selectivity ^b
	human nNOS	rat nNOS	human/rat
5	59	17	3.5
6	64	35	1.8
14a	425	139	3.1
14c	862	547	1.6
14g	84	43	2.0
14h	89	72	1.2
14j	13	16	0.8
14k	37	25	1.5

^a K_i values are calculated directly from IC_{50} values. IC_{50} values are the average of at least two replicates from nine data points. All experimental standard error values are less than 15%.

^bSelectivity values are determined by calculating the ratios of respective K_i values.

Table 3. Inhibition of human eNOS by compounds 5, 6, 14a, 14c, 14g, 14h, 14j, and 14k

Cmpd	K_i (nM) ^a		Selectivity ^b
	human eNOS	human nNOS	n/e
5	5006	59	85
6	6621	64	103
14a	18271	425	43
14c	42563	862	49
14g	73006	84	869
14h	22536	89	253
14j	22895	13	1761
14k	39533	37	1068

^a K_i values are calculated directly from IC_{50} values. IC_{50} values are the average of at least two replicates. All experimental standard error values are less than 15%.

^bSelectivity values are determined by calculating the ratios of respective K_i values.

Table 4. Percent inhibition of selected cytochromes P450 isozymes by 14j

	(% inhibition)			(% inhibition)	
	Positive controls ^{a, b}	14j ^a		Positive controls ^{a, b}	14j ^a
CYP1A2	95	9	CYP2C19	89	11
CYP2B6	98	8	CYP2D6	93	6
CYP2C8	95	2	CYP3A4	100	58
CYP2C9	98	0			

^aPerformed at 10 μ M concentration.

^bPositive control inhibitors are: Fluvoxamine (CYP1A2), Ticlopidine (CYP2B6), Quercetin (CYP2C8), Sulfaphenazole (CYP2C9), ticlopidine (CYP2C19), quinidine (CYP2D6), and ketoconazole (CYP3A4).

TOC Graphic

